A COMPREHENSIVE COUNTRY-SCALE DROUGHT MONITORING, THE NETHERLANDS

LUCIA GUARDAMINO
June, 2021

SUPERVISORS:
Dr. Z. Su
Dr. Y.Zeng
Dr. D. Rwasoka

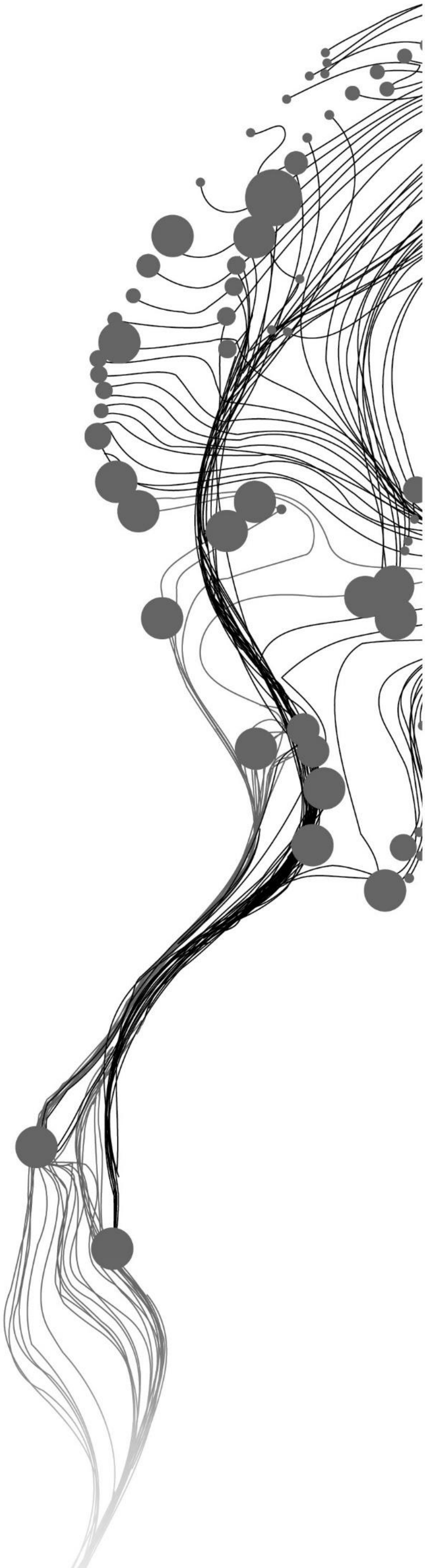

A COMPREHENSIVE COUNTRY-SCALE DROUGHT MONITORING,THE NETHERLANDS

LUCIA YESABELL GUARDAMINO SOTO
Enschede, The Netherlands, June, 2021

Thesis submitted to the Faculty of Geo-Information Science and Earth Observation of the University of Twente in partial fulfilment of the requirements for the degree of Master of Science in Geo-information Science and Earth Observation.
Specialization: Water Resources and Environmental Managament

SUPERVISORS:
Dr. Z. Su
Dr. Y.Zeng
Dr. D. Rwasoka

THESIS ASSESSMENT BOARD:
Dr. M. Lubczynski (Chair)
Dr. D. Hendriks, (External Examiner, Deltares)

ABSTRACT

In drought monitoring, some misinterpretations arise due to drought propagation over the water cycle involving one or more of its three dimensions: meteorological, soil moisture (SM) or agricultural, and/or hydrological. For instance, after a drought, increasing precipitation (meteorological dimension) usually does not have an immediate effect on the groundwater (hydrological dimension). Furthermore, while dry and wet anomalies have a strong effect over the meteorological dimension, evidenced by a higher variability and extreme changes, SM and groundwater (GW) show milder variations. Therefore, due to the lag effect and the smoother variations that mainly characterize the GW domain, drought over the SM and, primarily the GW, might persist even when the atmosphere switched from dry to wet anomalies.

This research applies a unified framework for drought monitoring in the Netherlands by analyzing the three drought components and their interactions using drought indices. Accordingly, a set of five indices were calculated, corresponding to precipitation (SPI, Standardized Precipitation Index), evapotranspiration (SPAEI, Standardized Precipitation and Actual Evapotranspiration Index, SPEI, Standardized Precipitation Evapotranspiration Index), SM (SSMI, Standardized Soil Moisture Index), and terrestrial water storage anomalies (STWSI, Standardized Terrestrial Water Storage Index).

A climatology dataset generated with the Terrestrial System Modeling Platform (TSMP) was used in the drought analysis. This dataset is the first high-resolution (12.5 km), long-term (1989-2019) terrestrial system climatology that includes an integrated simulation of the atmosphere, land surface, and subsurface over Europe. The dataset over the Netherlands was first validated from a qualitative and quantitative (Pearson correlation coefficient-*r* and *RMSE*) approach, followed by a spatio-temporal country-scale drought assessment from January 1989 to August 2019. The validation consisted of comparing TSMP variables (precipitation-PR, actual evapotranspiration-ETa, SM, and water table depth-WTD) with their in-situ counterparts. On the other hand, the spatio-temporal drought assessment was carried out at different time scales 1, 3, 6, 9, 12, and 24-month average. Consequently, three extreme droughts (1996, 2003, and 2018) were selected, and the patterns and physical processes were further analyzed. Critical areas to droughts were then determined based on the frequency and probability of extreme droughts (events where drought indices drop below -2).

We concluded that TSMP can provide a first approach to a comprehensive country-scale drought assessment in the Netherlands. The analysis indicates that TSMP is a robust dataset despite the different levels of agreement obtained for the WTD. Additionally, drought propagation is visible in the TSMP time series and shows a higher variability and intensity for PR and PR-ETa anomalies compared to SM and TWS anomalies. The time lag effect over SM and TWS is also visible in the temporal and spatial domains. On the other hand, based on the variables with the most extensive in-situ datasets (PR and reference evapotranspiration-ET0), we found that medium (9) to longer (24-month average) time scales have a higher *r* and lower *RMSE* when compared with the in-situ reference. This could be considered for future drought monitoring. Finally, we found that the TSMP performs better at defining the most susceptible areas to extreme droughts based on the long-term time series. Conversely, the performance is not so accurate at describing the development and intensities of separate extreme droughts such as 1996, 2003, and 2018.

ACKNOWLEDGEMENTS

I would like to thank my family because without them I would not be here. Thank you for your unconditional love, support and for encouraging me always.

My sincere gratitude to my supervisors Bob Su, Yijian Zeng, and Donald Rwasoka. Thank you for guiding me through this process under extraordinary circumstances. Professor Su and Yijian, I pretty much appreciate your insightful comments on every discussion, your explanations, and your patience. I also want to thank you for your quick responses, comments, and feedback. It really helped me to keep moving forward and conclude the thesis on time. Donald, thank you for your assistance with MATLAB at the beginning of the process. After that push, I was able to continue.

Special thanks to Carl Hartick and Carina Furusho from the Institute of Bio and Geosciences, Research Centre Jülich, for clarifying doubts and providing additional data required for the processing of the TSMP model outputs.

Thanks a lot to my mentor, Pr. Arno van Lieshout for your pieces of advice regarding our mental health and career development.

Special thanks to my seniors Lijie Zhang and Mostafa Gomaa, for your guidance during my studies and your support and advice with the thesis.

I would like to thank my friends, people who became my family at the ITC and who always supported me on every step during my master studies King, Boo, Cesar, Han, and Mateo.

I would also like to express my gratitude to Nestor for inspiring me and supporting me and his constant encouragement during this research.

Sincerely thanks to all my classmates and professors at the ITC, I learned a lot from all of you.

TABLE OF CONTENTS

1. Introduction 1

1.1. Background 1

1.2. Problem definition 2

1.3. Research objectives and questions 2

2. Study area 5

3. Data 8

3.1. In-situ data 8

3.2. Terrestrial System Modelling Platform dataset 9

4. Methodology 11

4.1. Data pre-processing 11

4.2. TSMP data assessment 11

4.3. Drought indices calculation 12

4.4. Country-scale drought assessment 14

5. Results 15

5.1. Performance of TSMP variables 15

5.2. Performance of TSMP derived drought indices 19

5.3. Country-scale drought assessment 23

6. Discussion 37

6.1. Feasibility of using TSMP data for a country-scale drought assessment in the Netherlands 37

6.2. Drought propagation 38

6.3. Response of droughts to physical processes 38

6.4. Critical areas to droughts 41

7. Conclusions 43

LIST OF FIGURES

Figure 1. Map of The Netherlands and delimitation of its provinces. 5

Figure 2. (a) PR, (b) Makkink ET0, and (c) T obtained from the 50 stations with completed and corrected data stored in the Klimatologish Informatie System. The linear trend for each variable is given by the corresponding equation. 6

Figure 3. (a) Elevations. Source: AHN3 - 5m, (b) Soil types. Source: Alterra, 2006. 7

Figure 4. In-situ stations selected for the validation of the TSMP dataset. 8

Figure 5. TSMP monthly ETa (mm/month) over Europe (March 2010). Negative values are associated with deposition (transformation of a gas into a solid). This phenomenon only takes place in winter. 9

Figure 6. Comparison between in-situ and TSMP PR at (a) 6.891E 52.274N, Eastern Netherlands (Overijssel province), (b) 5.873E 52.056N, Central Netherlands (Gelderland province), (c) 4.979E 52.644N, Western Netherlands (Noord-Holland province). 15

Figure 7. Comparison between in-situ ET0 and TSMP ETa at (a) 6.891E 52.274N, Eastern Netherlands (Overijssel province), (b) 5.873E 52.056N, Central Netherlands (Gelderland province), (c) 4.979E 52.644N, Western Netherlands (Noord-Holland province). 16

Figure 8. Comparison between in-situ and TSMP SM at (a) 6.921E 52.272N, Eastern Netherlands (Overijssel province), (b) 5.665E 51.710N, Southeastern Netherlands (Noord-Brabant province), (c) 4.790E 51.94N, Western Netherlands (Zuid-Holland). 17

Figure 9. Comparison between in-situ GWL and TSMP WTD at (a) 6.891E, 52.274N, Eastern Netherlands (Overijssel province), (b)5.680E 52.246N, Central Netherlands (Gelderland province), (c) 5.742E 50.908N, Southeastern Netherlands (Limburg province), (d) 5.862E 50.819N, Southeastern Netherlands (Limburg province), (e) 4.398E 51.552N, Southwestern Netherland (Noord-Brabant). 18

Figure 10. Comparison between short and long-term PR anomalies (SPI): (a,b) 6.891E 52.274N, Eastern Netherlands (Overijssel province), (c,d) 5.873E 52.056N, Central Netherlands (Gelderland province), (e,f) 4.979E 52.644N, Western Netherlands (Noord-Holland province). 21

Figure 11. Comparison between short and long-term ET anomalies (SPAEI-SPEI): (a,b) 6.891E 52.274N, Eastern Netherlands (Overijssel province), (c,d) 5.873E 52.056N, Central Netherlands (Gelderland province), (e,f) 4.979E 52.644N, Western Netherlands (Noord-Holland province). 22

Figure 12. Comparison between short and medium-term SM anomalies (SSMI): (a,b) 6.921E 52.272N, Eastern Netherlands (Overijssel province), (c,d) 5.665E 51.710N, Southeastern Netherlands (Noord-Brabant province), ... 23

Figure 13. Average country-scale time series at a short-term response (3-month average). 24

Figure 14. Average country-scale time series at a medium-term response (9-month average). 24

Figure 15. Average country-scale time series at a long-term response (24-month average).......................... 25

Figure 16. Maps of the 1996 event (a) hydrological drought onset, (b) meteorological drought onset, (c) maximum meteorological and hydrological drought, (d) hydrological drought end, (e) meteorological drought end. 28

Figure 17. Maps of the 2003 event (a) meteorological drought onset, (b) hydrological drought onset, (c) maximum meteorological drought, (d) meteorological drought end, (e) maximum hydrological drought, (f) hydrological drought end.. 31

Figure 18. Maps of the 2018 event (a) meteorological drought onset, (b) hydrological drought onset, (c) maximum meteorological drought, (d) maximum hydrological drought, (e) hydrological drought end, (f) meteorological drought end. 35

Figure 19. Frequency of extreme droughts in the Netherlands (index value <-2)... 36

Figure 20. Probability of extreme droughts in the Netherlands (index value <-2).. 36

Figure 21. Comparison of PR anomalies at a 9-month average between KNMI stations 48 (North) and 7 (SE). 39

Figure 22. Comparison of PR anomalies at a 9-month average between KNMI stations 40 (NE) and 7 (SE). 40

Figure 23. Comparison of PR anomalies at a 9-month average between KNMI stations 40 (NE) and 20 (Central).. 40

LIST OF TABLES

Table 1. Depth of each layer of the water column. Source: Research Centre Jülich..10

Table 2. Drought classification adapted from Mckee et al., (1993)...13

Table 3. Pearson correlation coefficient and RMSE of TSMP PR and PR anomalies compared to in-situ observations. 19

Table 4. Pearson correlation coefficient of TSMP ETa and ETa anomalies compared to in-situ observations. 19

Table 5. Pearson correlation coefficient and RMSE of TSMP SM and SM anomalies compared to in-situ observations. 20

Table 6. Pearson correlation coefficient of TSMP WTD compared to GWL in-situ observations. 20

Table 7. KNMI stations used in the interpretation of physical processes and identification of critical areas at a 9-month average. ID number of station corresponds to the NetCDF index of the data file. 42

1. INTRODUCTION

1.1. Background

Droughts have threatened societies throughout history and around the world. There is evidence of extreme droughts associated with the collapse of some civilizations, great famines, conflicts, and severe casualties (Su et al., 2017). In general terms, a drought can be defined as an insufficient amount of water in relation to the climatic average for a specific location and period (Su et al., 2017). The primary driver of droughts is a shortage of rainfall. However, anomalies in other climate variables such as evaporation and temperature (T) can also lead to drought conditions (Graw et al., 2019). Droughts are complex phenomena with multiple possible drivers that might interact with each other, operating at different spatial and temporal scales. Three types of droughts could be distinguished depending on the involved forcings: meteorological, SM or commonly known as agricultural, and hydrological (Su et al., 2017). Current anthropogenic climate change might increase the frequency and severity of this phenomenon with dramatic implications (Sivakumar et al., 2014). According to the High-level Meeting on National Drought Policy held in March 2013 (Geneva, Switzerland), in comparison with other hazards, droughts have long-term socio-economic effects with the most devastating impacts (Sivakumar et al., 2014).

Drought can be monitored by in-situ observations, remote sensing, and modeled datasets. Nowadays, several global and regional climate models are used in climate and hydrology, providing an improved spatially continuous and long-term coverage of hydrometeorological variables (El Kenawy et al., 2020). Regional climate models (RCMs) compared to Global Climate Models (GCMs) give more spatial details supporting the assessment of the phenomena, planning, and adaptation in smaller areas (CORDEX 2021).

Most GCM and RCMS simplify the SM and GW representation. In order to tackle this data/knowledge gap, the first long-term (September 1996 - August 2018, recently updated until August 2019), high resolution (~12.5km or 0.11°) terrestrial system climatology, was made available (Furusho-Percot et al., 2019). Also known as the Terrestrial System Modelling Platform (TSMP), this simulated dataset provides a comprehensive representation that includes the GW, land surface, and atmospheric systems. Additionally, the novelty of this dataset is the full 3D simulation of the GW and soil water dynamics, providing a complete picture of the water and energy cycles. The integration of GW data in climate analysis can lead to a better understanding of drought (Furusho-Percot et al., 2019).

Various drought indices were developed to characterize droughts and define their onset, duration, intensity, and geographic extent. An index is a single quantitative measure that translates one or several indicators (raw data) into a usable value. These indicators are associated with variables such as PR, evapotranspiration (ET), SM, etc. (Zargar et al., 2011). Droughts occur at different timescales, depending on the type of drought. This particular drought feature was considered in the design of the SPI, which is a widely used drought index. The SPI is a multi-scale index that eases the meteorological, agricultural, and hydrological drought analysis. Short-term responses to PR anomalies would be observed in the meteorological and agricultural dimensions (from around 1 to 6 months). In contrast, components of the hydrological dimension such as the streamflow, reservoirs, and GW would respond to longer PR anomalies (from around 6 to 24 months) (WMO, 2012). The long-term response of sub-surface water dynamics was also stated by a recent study that used this assumption to predict water conditions in 2020, after the drought of 2018 in Europe (Hartick et al., 2021). In order to get a physically consistent understanding of the meteorological, agricultural, and hydrological characteristics of drought and their interplays, it is suggested to put different drought indices from these dimensions into one common framework for analysis and assessment (Su et al., 2017).

This study consists of two parts. In the first part, TSMP (hereinafter referred as the data outputs of the TSMP modeling system) was verified against in-situ observations. PR, ETa, SM, and WTD time series were evaluated with equivalent or similar in-situ observation for the period January 1989 to August 2019. Corresponding indices were also calculated and validated. In the second part, a drought assessment for the Netherlands was conducted for the same period. The drought assessment consisted of analyzing the country-scale temporal responses, which allowed the identification and further assessment of three significant droughts that occurred in the Netherlands in 1996, 2003, and 2018. The analysis of the probability of occurrence of extreme droughts followed, identifying the most susceptible areas in the Netherlands to droughts over the period January 1989 to August 2019.

A set of indices representing different water cycle components (PR, ETa, ET0, SM, and WTD) were selected. The indices are SPI, SPAEI, SPEI, SSMI, and STWSI.

1.2. Problem definition

Previous research has mainly focused on analyzing some variables or components of drought events: meteorological, agricultural, or hydrological, instead of studying the whole water system (e.g., considering the water cycle including GW dynamics).

Droughts are events that develop over an extended period, and sometimes one can see controversial signals from different drought indices. For example, after some heavy rainfalls, the grass could turn green while the groundwater table might remain low, indicating that the drought continues (KNMI, 2020). Research shows that GW may be highly susceptible in a scenario of a prolonged drought, taking longer to recover compared to surface water reservoirs (Bloomfield & Marchant, 2013). Because the three types of droughts operate at different spatial and temporal scales, it is essential to evaluate droughts from a holistic perspective using multiple indices (Maina, 2018; Su et al., 2017) and by considering the multidimensional characteristic of this phenomenon (Zargar et al., 2011). Following this approach, a misinterpretation of an event could be prevented. For instance, by detecting a drought by one index that could be ignored by others.

1.3. Research objectives and questions

1.3.1. Main objective:

The objective of this study was to carry out a comprehensive country-scale drought analysis in the Netherlands from January 1989 to August 2019.

1.3.2. Sub-objectives and research questions

The main objective was achieved by defining three sub-objectives and the corresponding research questions.

Sub-objective 1: To validate the TSMP simulation with in-situ observations.

- Does the time series of the PR, ETa, SM, and WTD from the TSMP resemble in-situ observations?

- Does the time series of the TSMP anomalies (i.e. standardized indices) resemble the anomalies from the in-situ observations?

Sub-objective 2: To derive a set of drought indices from the meteorological, agricultural, and hydrological dimensions and understand their spatio-temporal responses and connections.

Sub-objective 3: To carry out a country-scale drought analysis.

- What were the average country-scale temporal responses of the indices for the whole country?
- What were the spatial responses of the indices for selected drought events?
- Were there areas with a higher probability of extreme droughts in the Netherlands?
- Are there some sensitive areas to droughts in the Netherlands?

2. STUDY AREA

The Netherlands is situated in Northwestern Europe. It lies between latitudes 50˚ 71' to 53˚ 79'N and longitudes 3˚28' to 8˚05'E (Figure 1). This country is located within a delta and characterized by a flat topography. As a result, two-thirds of the land area is below sea level, making this country prone to floods. However, with climate change, droughts are becoming a new threat and challenge for water managers (Weijers, 2020).

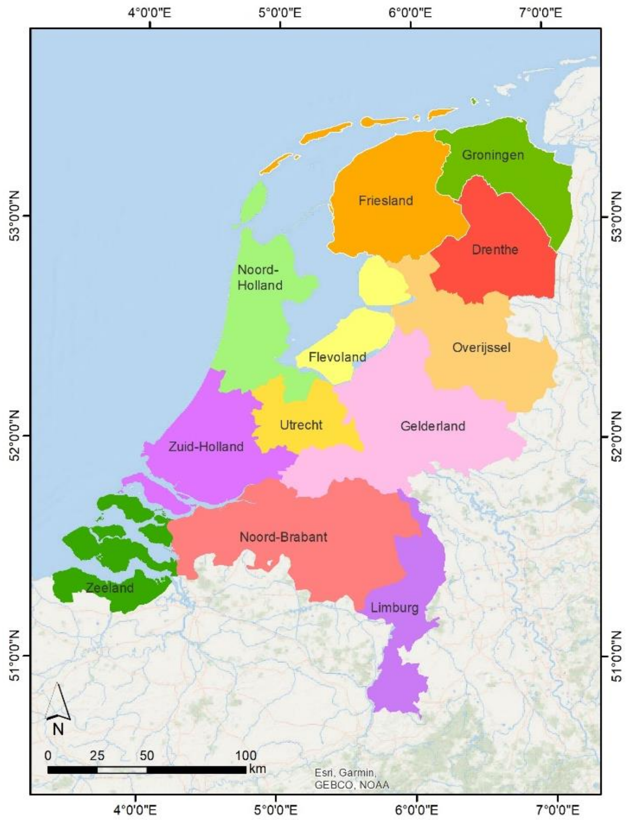

Figure 1. Map of The Netherlands and delimitation of its provinces.

Extreme drought was experienced in the summer of 2018, while 2019 and 2020 were drier than average (KNMI, 2020). The impact of droughts was not uniform across the country. According to Philip et al., (2020), despite an even rise in T in the Netherlands, solar radiation was slightly higher inland, while more PR was observed on the coast. With no increasing PR, a higher ET rate due to higher T, and a water supply that mainly relies on rainfall, the interior of the country would be more susceptible to drought.

An estimation based on the stations of the Klimatologisch Informatie System (KIS, KNMI) for the period 1951-2020 (PR and T) and 1957-2020 (ET0) indicates that PR, T, and ET0 show positive trends. The trend is more significant for ET0 and T, which makes sense considering that these two variables are linked (Figure 2).

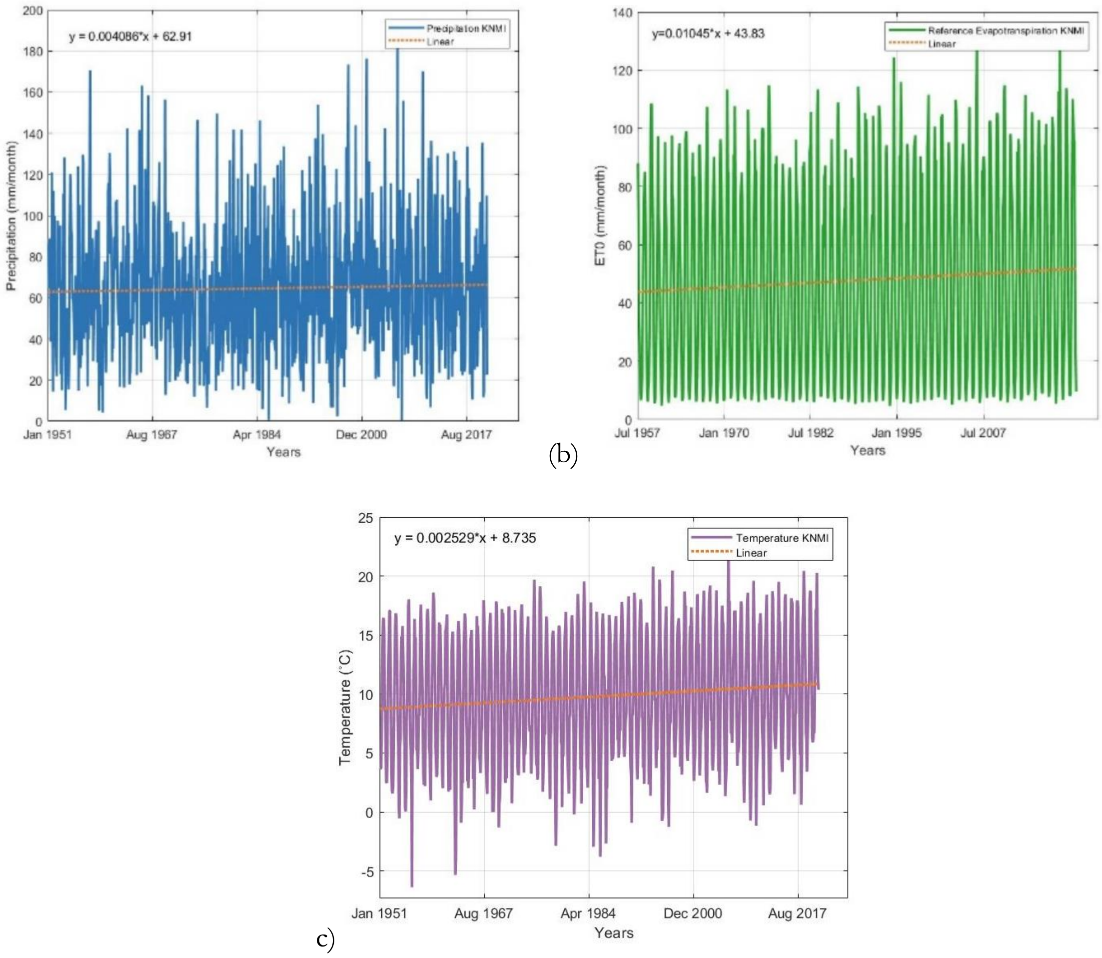

(a) (b) c)

Figure 2. (a) PR, (b) Makkink ET0, and (c) T obtained from the 50 stations with completed and corrected data stored in the Klimatologish Informatie System. The linear trend for each variable is given by the corresponding equation.

The Actueel Hoogtebestand Nederland or the Current Elevation File of the Netherlands (AHN3) obtained from the Nederlands Hydrologish Instrumentarium (NHI) indicates that on average, the topography in the East of the country (from North to South in the provinces of Drenthe, Overijssel, Gelderland, the East of Utrecht, North Brabant, and Limburg) is higher than that in the West. The highest peaks (approximately ≥ 100 m.a.s.l.) are found in the Southeast (SE), in the province of Limburg. In the central part of the country, to the Northwest of Gelderland, it is located the second more important elevated area reaching altitudes around 80 and 100 m.a.s.l. The provinces of the North and West (Groningen, Friesland, Flevoland, North and South Holland, and Zeeland) are predominantly below the sea level or reach lower altitudes up to 10m. Particularly, the province of Flevoland lies entirely below sea level (Figure 3a).

The land use map obtained from the Nederlands Hydrologish Instrumentarium (NHI) show that grasslands represent the primary land use in the country, prevailing in the provinces of the inland area: Overijssel, Gelderland, Utrecht, and North Brabant, and in the coastal province of Friesland. These provinces are also dedicated to the cultivation of maize on a smaller scale. Agriculture is an important land use activity as well. In provinces such as Flevoland, Zeeland, and near the Northeastern border of the country between Groningen and Drenthe, the cultivation of cereals and potatoes is a primary or secondary land use activity. Compared to other provinces, the urban land use is remarkably more extensive in the coastal area in South and North Holland. In contrast, the largest coniferous and deciduous forest is located in the Northwest of Gelderland, coinciding with the location of the second most elevated area of the country.

The soil type map was obtained from the Dutch Soil Information System (BIS-Nederland, Alterra), and it contains ten major soil units. Inland is mainly characterized by sandy soils, while the coastal zone is primarily constituted by light loam and clay and heavy clay and sludge soils (Figure 3b). The GW table in the Netherlands (NHI) indicates that groundwater levels (GWL) vary from -10 to >10 m with respect to the surface level. The groundwater table is deeper inland than in the coastal region.

a)
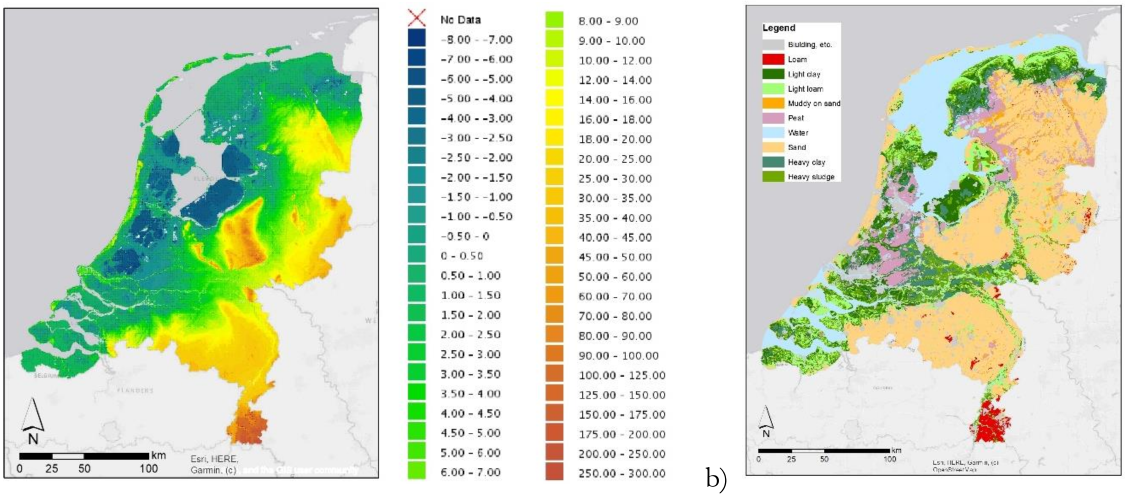

b)

Figure 3. (a) Elevations. Source: AHN3 - 5m, (b) Soil types. Source: Alterra, 2006.

3. DATA

3.1. In-situ data

PR and ET0 calculated by the Makkink method were obtained from the Koninklijk Nederlands Meteorologish Instituut (KNMI). The KNMI stores validated (completed and corrected) meteorological data in the KIS. PR data is available on a daily timescale from January 1951 to the present, whereas ET0 data is available from July 1957 to the present. These data can be freely accessed in a NetCDF file format through the KNMI data platform (https://dataplatform.knmi.nl/catalog/datasets/index.html?x-dataset=etmaalgegevensKNMIstations&x-dataset-version=1). Three stations with PR and ET0 data were selected for the analysis (Figure 4).

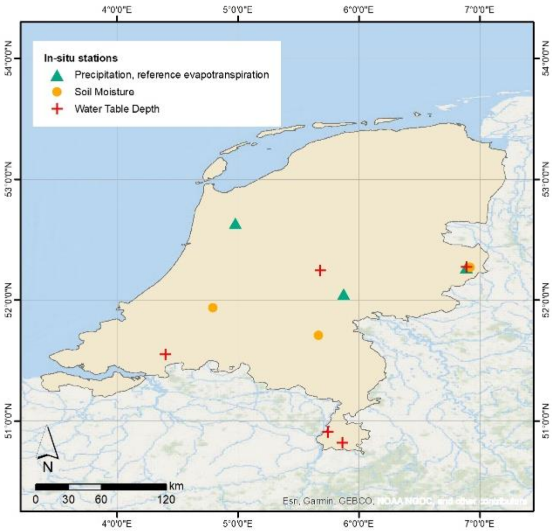

Figure 4. In-situ stations selected for the validation of the TSMP dataset.

SM data at 5cm depth was obtained from the Twente (Dente et al., 2011; Van Der Velde et al., 2021) and Raam (Benninga et al., 2018) regional SM networks, where the stations ITCSM_04 and RM_SM_09 were respectively selected. The selection of the stations was based on the completeness of the data. Data from the ITCSM_04 station is available from January 1st, 2015 to the present, and the RM_SM_09 station is available from April 5th, 2016 to the present. Both datasets are provided at a 15-minute time interval. Data from the Twente network is open to the public upon request (https://easy.dans.knaw.nl/ui/datasets/id/easy-dataset:130209), while SM data from the Raam network can be freely accessed through the link: https://research.utwente.nl/en/publications/the-raam-regional-soil-moisture-monitoring-network-in-the-netherl/datasets/. Additionally, the station with code 3sh9gmem was downloaded from the GROW network available in the International Soil Moisture Network (ISMN, https://www.geo.tuwien.ac.at/insitu/data_viewer/) portal. In contrast to the other two regional datasets located in the inland region, this station was selected because it is located on the coastal side. The ISMN station provides hourly data at a 10 cm depth from July 2018 to June 2019 (Figure 4).

GWL were retrieved from the open-access DINOloket's database (https://www.dinoloket.nl/ondergrondgegevens) in a CSV format. DINOloket is a Dutch geoscientific portal developed and managed by the TNO Geological Survey of The Netherlands. This platform is a central collector of the deep and shallow subsurface of the Netherlands. Data from five measurement points were downloaded from the data portal (Figure 4). The frequency among measurements is around 14 days, meaning that approximately two measurements are available every month.

3.2. Terrestrial System Modelling Platform dataset

The TSMP version 1.1 is the first high-resolution (0.11˚ or ~12.5km), long-term (1989-2018) (recently updated until 2019) simulated terrestrial climatology over Europe that provides a complete representation of the water cycle. In contrast to most RCMs, TSMP simulates the interaction between the different water cycle components, including SM and GW (Furusho-Percot et al., 2019).

TSMP is a fully coupled model that consists of the weather prediction model COSMO version 5.01, the land surface model CLM version 3.5, and the surface-subsurface hydrologic model ParFlow version 3.2. The Ocean Atmosphere Sea Ice Soil (OASIS3) Model Coupling Toolkit (MCT) was used as an external coupler to integrate the three models. The dataset provides daily data from January 1989. However, some cells reach the GW equilibrium in 1995, making data from 1996 appropriate for the analysis (Furusho-Percot et al., 2019).

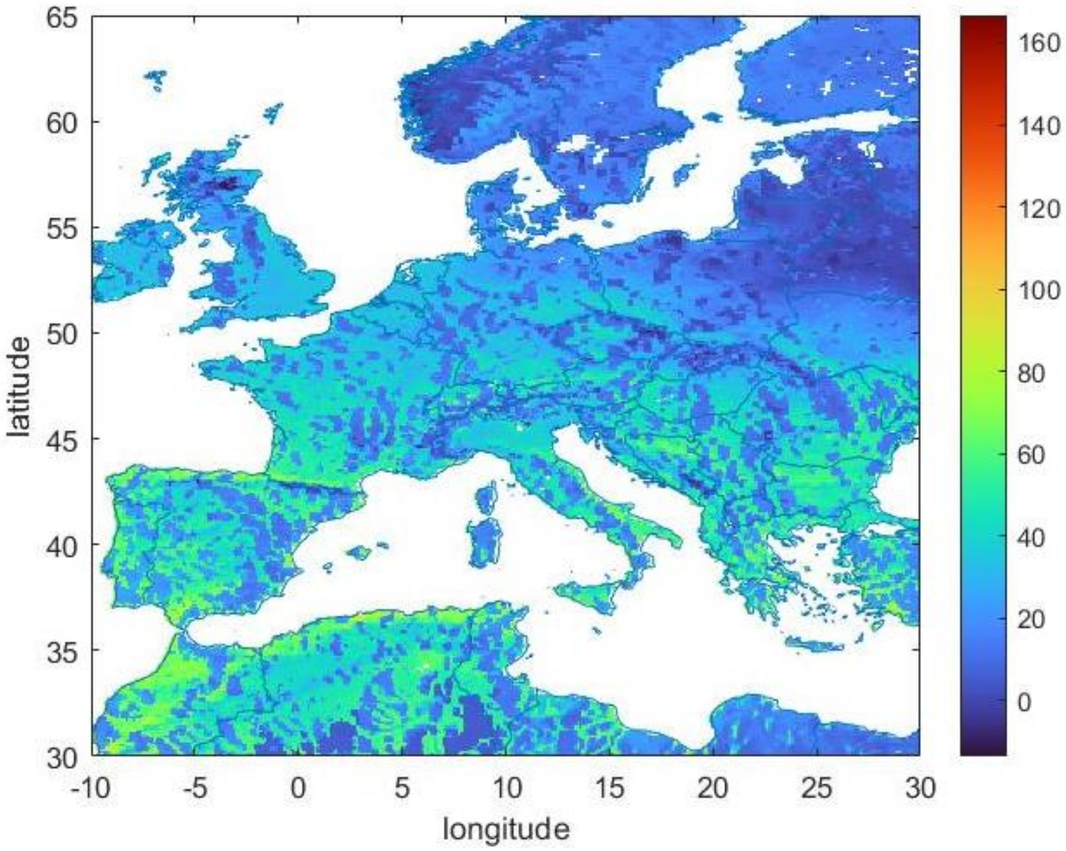

Figure 5. TSMP Monthly ETa (mm/month) over Europe (March 2010). Negative values are associated with deposition (transformation of a gas into a solid). This phenomenon only takes place in winter.

The TSMP data outputs were set up following the modelling protocol of the Coordinated Regional Downscaling Experiment (CORDEX). The EUR-11 grid was used (0.11˚) together with rotated latitude and longitude coordinates, representing 412 × 424 grid cells. Over the vertical dimension, the data consists of 15 layers and a total depth of 57 meters from the surface to the aquifer (Table 1) (Furusho-Percot et al., 2019; Hartick et al., 2021).

Table 1. Depth of each layer of the water column. Source: Research Centre Jülich.

Layer	Depth - Dz(m)
15	0.02
14	0.03
13	0.05
12	0.07
11	0.13
10	0.2
9	0.3
8	0.5
7	0.7
6	1
5	4
4	10
3	10
2	15
1	15
Total	57

The variables from the dataset employed in the analysis were: PR, ETa, soil-groundwater saturation (SGW), and WTD. The data can be downloaded from: https://datapub.fz-juelich.de/slts/cordex/data/.

A porosity file in NetCDF format that covers the European CORDEX domain was provided by the Research Centre Jülich. It consists of one layer over the vertical dimension that follows the EUR-11 grid CORDEX setup.

4. METHODOLOGY

4.1. Data pre-processing

The period selected for the analysis was January 1st, 1989 to August 31st, 2019. Thus, the data contained within this time frame was extracted and used for further analysis. After extracting the required data, in-situ PR and ET0, retrieved from the KNMI (PR and ET0), data from the regional SM networks, and the GWL from DINOloket were aggregated to a monthly time scale using MATLAB R2020b.

The TSMP NetCDF files were mostly pre-processed using CDO version 1.9.4. The multiple TSMP files corresponding to every year were first combined into one single file. A rotation of the coordinates was then applied using the nearest neighborhood remapping method in order to preserve the original values as much as possible. Later, the files were subset to the area of the Netherlands and aggregated from a daily to a monthly time scale. An additional step was applied to the ETa before the aggregation to convert the units from mm s^{-1} to mm day^{-1}. In the case of PR, the aggregation was carried out in MATLAB after converting PR values from cumulative (PR from a specific day plus the cumulative PR of the previous days) to actual daily values. Both in-situ data and TSMP data were selected for the period January 1989 to August 2019.

4.2. TSMP data assessment

The data assessment involved a qualitative and a quantitative analysis, and it was applied for the absolute values (PR, ET0, SM, and WTD) and the anomalies (SPI, SPAEI-SPEI, SSMI, STWSI).

A pixel-station comparison was carried out between TSMP and selected in-situ data points in different geographic areas across the country (Figure 4). The qualitative assessment consisted of plotting together the time series of both datasets. Then, a visual inspection was applied with an emphasis on observing the seasonality of the data and the detection of dry and wet periods (occurrence, intensity, and duration). On the other hand, two statistic metrics were applied for the quantitative analysis: the Pearson Correlation Coefficient (*r*) and/or the Root Mean Square Error (*RMSE*). *RMSE* was only applied to the variables with the same physical measurement, such as PR and SM. The statistic metrics were calculated at 1, 3, 6, 9, 12, and 24-month average for PR and ET. Regarding SM, due to the short data availability, the static metrics were only calculated for short (1, 3, 6-month average) and medium time scales (9-month average).

The KNMI does not measure ETa, nonetheless ET0 was used as a reference to determine if the values provided by TSMP made sense. In principle, ET0 should be higher than ETa.

In order to validate the Terrestrial Water Storage (TWS) in the aquifer, a comparison was applied in the GW component between the WTD variable provided by TSMP and the GWL from DINOloket. Then, for SM validation (first 5cm or 10 cm below the surface), it was required to estimate the TWS in the top layers representing the soil water storage. $TWS_{i,j}$ is an integrated indicator of water resources and was derived from the modeled relative saturation data $SGW_{i,j,k}$ (-), and the porosity $\emptyset_{i,j,k}$ (-) for a pixel with indices i,j (over the horizontal dimension), and k (over the vertical dimension). The vertical extent of each layer and the number of grid cells in the vertical dimension was represented by dz_k(L) and nz (Eq. 1). The porosity was considered homogeneous over the 15 layers (Hartick et al., 2021).

$$TWS_{i,j} = \sum_k^{nz} SGW_{i,j,k}\ \emptyset_{i,j,k} dz_k \quad (1)$$

SM values were extracted from the first two (5cm) and three (10cm) top layers of the TWS (layers 13, 14, and 15 of TSMP, see Table 1) and later compared to SM measurements of the ISMN, and the Twente and Raam regional networks.

The quantitative assessment consisted of calculating the *r* coefficient and *RMSE*. Both are widely used metrics applied for the comparison between modeled (x_{mod}) and observed (x_{obs}) data (Furusho-Percot et al., 2019; Zhang, 2020). The mathematical expressions of *r* and *RMSE* can be found in Eq.2, and 3, respectively.

$$r = \frac{\sum(x_{mod}-\overline{x_{mod}})(x_{obs}-\overline{x_{obs}})}{\sqrt{\sum(x_{mod}-\overline{x_{mod}})^2(x_{obs}-\overline{x_{obs}})^2}} \tag{2}$$

$$RMSE = \sqrt{\frac{\sum_i^N (x_{mod}-x_{obs})^2}{N}} \tag{3}$$

Likewise, the performance of the TSMP anomalies was also assessed in contrast to the in-situ anomalies. For ET, similar but not the same indices were calculated. Therefore, the SPAEI (PR-ETa) derived from TSMP was compared to SPEI (PR-ET0) derived from the in-situ observations. Regarding TWS, no in-situ measurements were available. Hence the STWSI estimated from TSMP was not compared with an in-situ counterpart.

4.3. Drought indices calculation

Furusho-Percot et al., (2019) recommended constraining the TSMP period suitable for analysis from 1996 onwards since GW completely reached equilibrium for some cells in 1995. After making plots of TSMP variables PR, ET0, SM, and WTD with their in-situ counterparts, no significant differences were observed in the performance of the data before and after 1995. Moreover, drought assessments require a minimum of 30 years to ensure that the confidence of the results is acceptable (Mckee et al., 1993; WMO, 2012). After pondering these two aspects, drought indices were generated for the whole TSMP time series (January 1989 – August 2019).

A set of five standardized indices were selected to assess the meteorological, SM, and hydrological drought: SPI, SPAEI, SSMI, and STWSI. Standardized indices were used because it enables the comparison between different indices (Su et al., 2017). An additional ET index (SPEI) was also calculated to evaluate the performance of the SPAEI obtained from TSMP. The indices were calculated for 1, 3, 6, 9, 12, and 24-month average, which are the most used time scales (WMO, 2012).

4.3.1. Standardized Precipitation Index

The SPI was first introduced by Mckee et al. (1993). The calculation of this index relies only on PR, making this index relatively simple to obtain. The SPI estimation requires four steps: (1) moving average estimation over the time window of 1, 3, 6, 9, 12, and 24 months, thus for each month, a new value is calculated based on the previous and next(s) month(s), (2) fit the climatic record to a gamma probability distribution function, (3) use the parameters to obtain the cumulative density distribution function, (4) estimate an inverse normal distribution using the general standardization equation (Eq. 4) where x_i is the PR variable, $\bar{x}$ is the average for that specific month over the whole dataset, and $\sigma(x)$ is the standard deviation of that specific month compared to all the months of the whole period.

$$\frac{x_i - \bar{x}}{\sigma(x)} \tag{4}$$

The SPI represents the number of standard deviations that the cumulative PR deficit deviates from the normalized long-term average (Maina, 2018; Su et al., 2017). A drought event starts when the SPI consistently shows a value below zero and ends when it reaches a positive value after drop to -1.0 or less. Drought intensity is illustrated in Table 2.

Table 2. Drought classification adapted from Mckee et al., (1993).

SPI values	Drought category
≥ 2.00	Extremely wet
1.5 to 1.99	Severely wet
1 to 1.49	Moderately wet
0.5 to 0.99	Slightly wet
-0.49 to 0.49	Near Normal
-0.99 to -0.5	Slightly dry
-1.00 to -1.49	Moderately dry
-1.50 to -1.99	Severely dry
≤ -2.00	Extremely dry

4.3.2. Standardized Precipitation and Actual Evapotranspiration Index and the Standardized Precipitation Evapotranspiration Index

The SPAEI is a relatively new index compared to the widely used SPEI. However, SPAEI may be a more suitable index for drought monitoring. SPEI estimation is based on the difference: PR-PET (Potential Evapotranspiration), meaning that it represents the energy-based atmospheric water demand, excluding the influence of regional land surface changes and actual moisture availability which is given by PR–ETa. On the contrary, ETa is an indicator of the transfer of moisture from the surface to the atmosphere as a result of the energy demand and available moisture supply (Rehana & Monish, 2020). Moreover, in a study developed in Thailand, SPEI unsuccessfully depicted extreme droughts in the period 1993 – 1994. Instead, it indicated a slightly delayed dry period. Whereas SPAEI clearly represented the intensification of the drought event (Homdee et al., 2016).

In order to calculate the SPAEI, the water deficit was first estimated based on the difference between PR - ETa, as explained before. Then it followed the SPI four-step protocol with the difference that the climatic record was fitted to a Generalized Extreme Values (GEV) probability distribution. The GEV was adopted because it allows negative values, which can be the case if ETa or the PET are higher than PR. Furthermore, the GEV makes an adequate representation of the extremes and has the best goodness of fit over different monthly timesteps (Maina, 2018; Stagge et al., 2015). SPEI calculation followed the same steps as SPAEI with the distinctness that it results from the difference between PR – ET0. Drought was classified following the categorization presented in Table 2.

4.3.3. Standardized Soil Moisture Index and the Standardized Terrestrial Water Storage Index

The TWS is an integrated measurement of all the water cycle components over and beneath the land surface: GW, SM, snow and ice, canopy water storage, overland flow, etc. In this study, TWS represents the aggregation of GW and SM. After the moving average calculation over a 1, 3, 6, 9, 12, and 24 months timestep, a standardization procedure was applied as indicated in Eq. 5. SM was calculated using the same equation with the difference that it only took into account two (the top 5 cm) or three layers (the top 10 cm) (Table1). See Eq. 6. Drought was classified following the categorization presented in Table 2.

$$STSWI_{ijk} = \frac{TWSI_{ijk} - \overline{TWSI_{ijk}}}{\sigma_{ij}} \quad (5)$$

$$SSMII_{ijk} = \frac{SSMI_{ijk} - \overline{SSMI_{ijk}}}{\sigma_{ij}} \quad (6)$$

4.4. Country-scale drought assessment

First, the average country-scale temporal responses were calculated for all the standardized indices in the period January 1989 – August 2019. Secondly, the most significant drought events were selected: 1996, 2003, and 2018. Then, a series of maps were generated to observe the evolution of the meteorological, SM, and hydrological drought. The criteria followed to plot the maps consisted of:

a) Mapping the months with the onset, maximum dry conditions, and end of the meteorological and hydrological drought. These two types of droughts were selected as a reference due to their respective fast and slow response to water deficit. Therefore, the whole duration of drought in the water cycle could be covered.
b) Defining a drought onset from the month that continuous negative values were recorded, consequently dropping to -1 or less. A drought ends when it reaches a positive value.
c) Elaborating the maps based on the onset, maximum dry conditions, and end estimated by a 9-month average. This timescale was chosen because it represents a medium-term response.
d) Generating the maps using a stepwise interval: 3, 6, 9, and 12-month average.
e) Cutting the analysis period until March 2019 (for the 2018 drought) based on the longer time window (*n=12*). When the time window *n* is >1, the average is calculated only for the available values at the endpoints. Either *n* is an odd or even number, the sliding window truncates for the first *n/2* values at the beginning of the time series and for the last *(n/2)-1* values at the end of the time series. For instance, in a window of a 12-month average (*n=12*), the first moving average value only averages the first six values, the second one, the first seven values, and so on until reaching the 7th value where a standard calculation over 12 values starts. At the end of the time series, the last five months are progressively averaged over 11, 10, 9, 8, and 7. Therefore, only in the endpoints there is a gradual increasing uncertainty.

Finally, a series of maps with the frequency of extreme drought events (i.e., months with values ≤-2) was developed for the whole period and for every index: SPI, SPAEI, SSMI, STWSI, at different time scales: 3, 6, 9, and 12-month average. Then, the probability of extreme droughts was calculated by dividing the frequency over the total number of months (i.e., 368 months).

5. RESULTS

5.1. Performance of TSMP variables

5.1.1. Precipitation

The qualitative inspection indicates that overall there is a good agreement between in-situ and modeled TSMP data. The time series of both datasets were plotted for three selected geographic points of the Netherlands: East (Overijssel), Central (Gelderland), and West (Noor-Holland) (Figure 4). According to the observations, TSMP PR shows some clear underestimations, which are more evident in the West (e.g., August 2014 and September 2017). The West shows a relatively higher difference between model and in-situ data compared to the East and Central points. The higher disagreement in the West is also reflected in the moderately low *r* coefficient (0.46) and higher *RMSE* (39.10 mm/month). Additionally, for the three analyzed points, the upwards spikes seem to be better represented than the downwards spikes (Figure 6, Table 3).

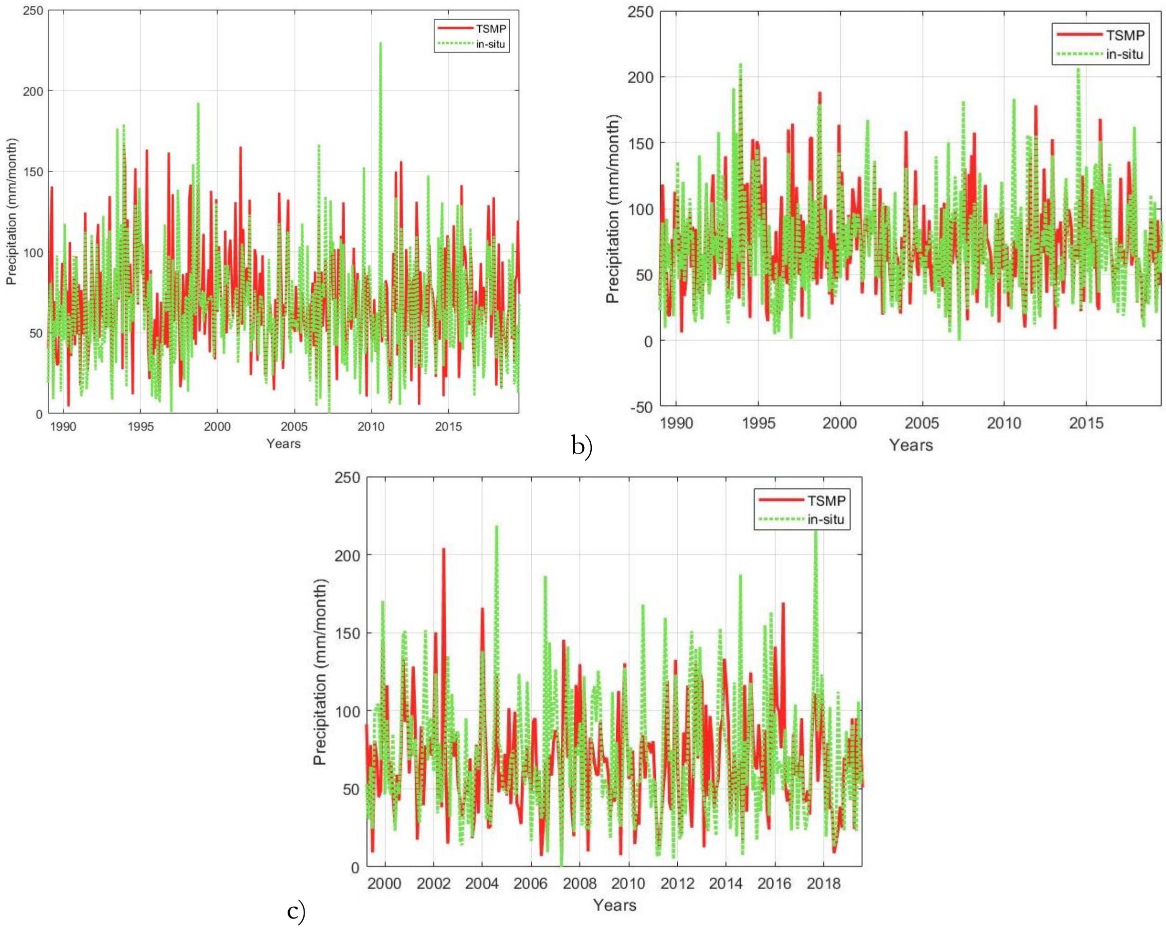

a) b) c)

Figure 6. Comparison between in-situ and TSMP PR at (a) 6.891E 52.274N, Eastern Netherlands (Overijssel province), (b) 5.873E 52.056N, Central Netherlands (Gelderland province), (c) 4.979E 52.644N, Western Netherlands (Noord-Holland province).

5.1.2. Evapotranspiration:

The consistency of the TSMP ETa was assessed by looking into the provided ET0 from the KNMI (Figure 4). The modeled ETa kept below ET0 values in the three assessed stations. Modeled data also captured well the seasonality with periods of higher and lower ET. It also corresponds with really good *r* coefficients

>0.90 for the three assessed points (Table 4). However, both datasets evolved differently regionally. While in-situ ET0 does not show significant differences among the three evaluated locations, TSMP ETa presents clear dissimilarities. For instance, the point located closer to the coast exhibits higher ETa values (>60 mm/month), probably due to higher SM (Figure 7c). On the other hand, the point taken from the central part presents lower ETa (<40 mm/month) (Figure 7b).

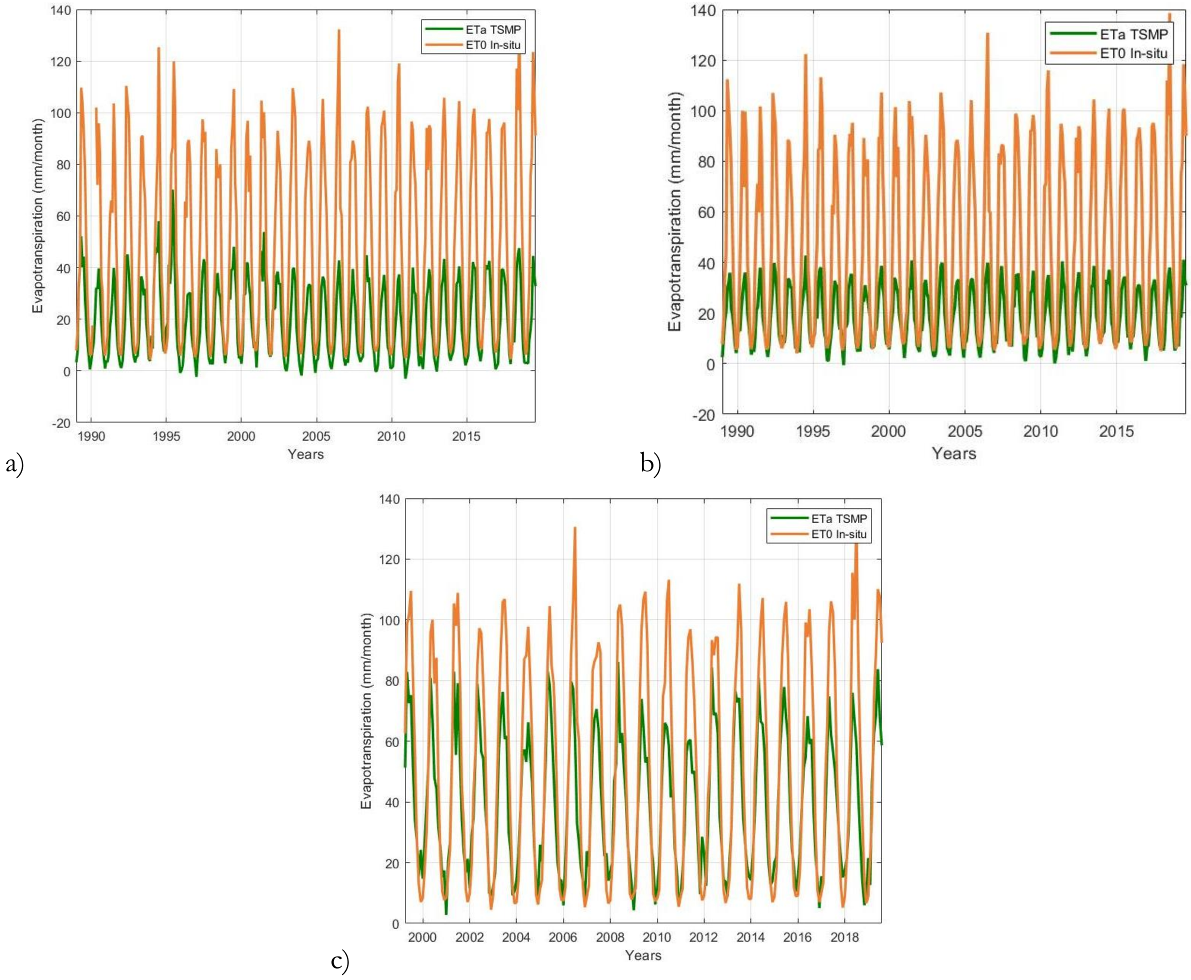

Figure 7. Comparison between in-situ ET0 and TSMP ETa at (a) 6.891E 52.274N, Eastern Netherlands (Overijssel province), (b) 5.873E 52.056N, Central Netherlands (Gelderland province), (c) 4.979E 52.644N, Western Netherlands (Noord-Holland province).

5.1.3. Soil moisture

Compared to other variables, in-situ SM measurements were available for a short period. The longest time series was provided by the Regional SM network of Twente in the Overijssel province from January 2015 to August 2019. The network located in the Raam catchment (Noord-Brabant) started to measure in April 2016, and the data was available until April 2019. The station from the ISMN located in Zuid-Holland measured for less than a year, from July 2018 to June 2019. The data from the regional networks were taken at 5cm depth, while the station from the ISMN only provided data at 10cm depth (Figure 4).

In general, the representation of the SM dynamics was quite good at 5 and 10cm depth, with moderate to high *r* coefficients (0.57 to 0.88). The highest *r* coefficient was obtained in Zuid-Holland at 10cm depth with 0.88, followed by the simulation of the reference station points of the Overijssel and Noord-Brabant provinces. Likewise, the representation of the magnitude was closer in the Zuid-Holland station (0.10 m^3/m^3) and further in the Noord-Brabant station (0.13 m^3/m^3) (Figure 8, Table 5).

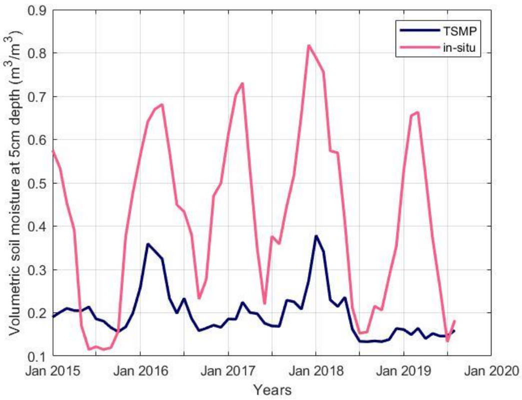

a)

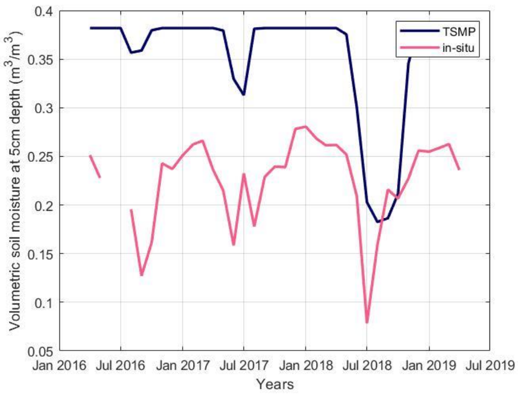

b)

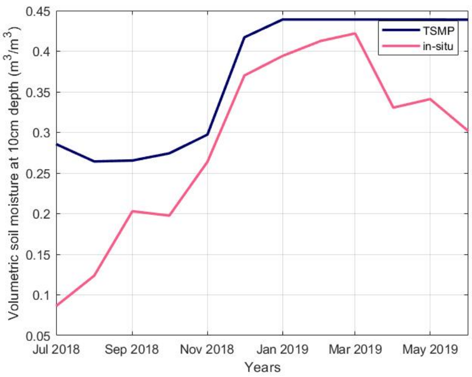

c)

Figure 8. Comparison between in-situ and TSMP SM at (a) 6.921E 52.272N, Eastern Netherlands (Overijssel province), (b) 5.665E 51.710N, Southeastern Netherlands (Noord-Brabant province), (c) 4.790E 51.94N, Western Netherlands (Zuid-Holland).

5.1.4. Water table depth

The WTD (m below the land surface) was compared to existing GWL observation from DINOloket (height m from the NAP reference). Five points were taken to assess the performance of the data in the period (1989-1995) (Figure 4). As mentioned in Section 3.2, some cells in the TSMP model reached equilibrium in 1995. Therefore, the period suitable for analysis would be from 1996 (Furusho-Percot et al., 2019). The visual inspection suggests that the performance of the data in the period after 1995 is not necessarily better than that in the period 1989-1995 (Figures 9b, c, d, e).

On the other hand, the simulation was closer to actual observations for some stations than others. For example, the simulations from the East and Southwest (SW) present a better fit, with *r* coefficients of -0.56 in both cases. In contrast, the Central and Southeastern assessed points got pretty low *r* coefficients of -0.21, -0.38, and 0.04, the last two values corresponding to the SE. Negative *r* coefficients are associated with the units of WTD (m below the surface) and GWL (m with respect to the NAP reference, which is zero), meaning that increasing WTD corresponds to decreasing GWL and vice versa (Table 6).

By looking at the time series of the Central point, we can observe that TSMP exhibits a higher variability than the in-situ observations. Nonetheless, the representation seems not to be far. Wet and dry periods are mostly captured with the difference that the in-situ observations have a smoother effect (Figure 9b).

Moreover, it is interesting that the two SE geographic points present a different performance (Figures 9c, 9d). Despite in both cases, an almost flat pattern can be visualized in the highest peaks. In Figure 9c, the wet and dry dynamics are still represented. Conversely, Figure 9d exhibits a pretty bad performance, even from the qualitative perspective, with an almost contradictory simulation of the actual observations.

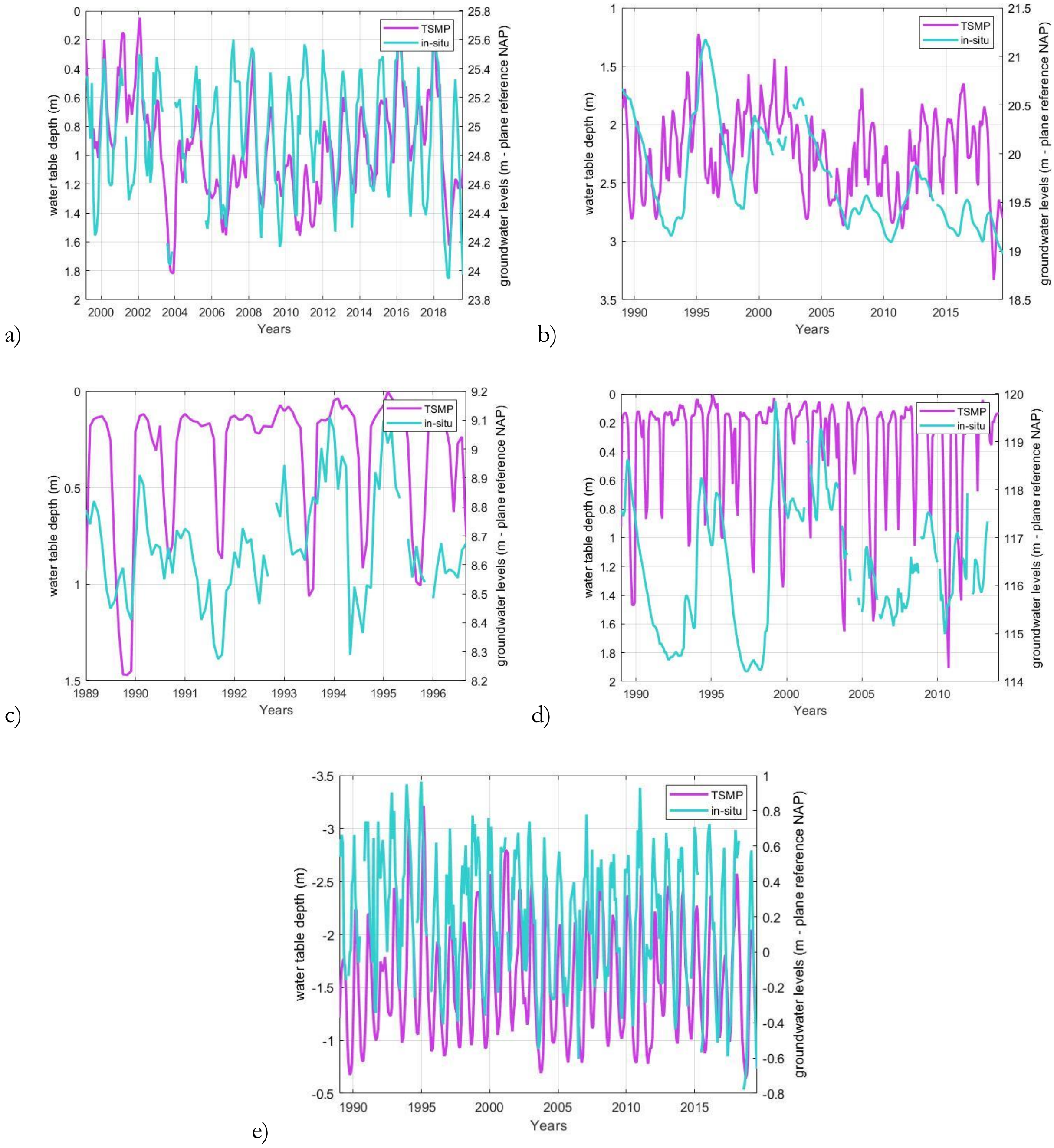

Figure 9. Comparison between in-situ GWL and TSMP WTD at (a) 6.891E, 52.274N, Eastern Netherlands (Overijssel province), (b)5.680E 52.246N, Central Netherlands (Gelderland province), (c) 5.742E 50.908N, Southeastern Netherlands (Limburg province), (d) 5.862E 50.819N, Southeastern Netherlands (Limburg province), (e) 4.398E 51.552N, Southwestern Netherland (Noord-Brabant).

5.2. Performance of TSMP derived drought indices

Drought indices calculated for shorter timescales (e.g., 1 or 3-month average) indicate frequencies of more dry or extremely dry periods. When the timescale increases, the frequency reduces, and the duration of the wet and dry periods prolongs.

Two extremely dry periods can be particularly identified from the SPI time series (1996 and 2018), considering both model and in-situ observations. However, some regional differences in the performance of the TSMP data can be visualized. For example, the event of 1996 was better represented by the Eastern station (Figure 10a, b), while in the Central station, the breach of the representation progressively increased and became more remarkable at a 12 and 24-month average (Figure 10c, d). Since the in-situ records of the Western station are available from 1999, the period before this year was not simulated, including the event of 1996. The 2018 simulation more or less reflects actual observations in the three stations. Another relatively significant drought is the one developed in 2003, but it is more important at shorter time scales such as 3 and 6-month average (Figure 10 a, b).

Table 3. Pearson correlation coefficient and RMSE of TSMP PR and PR anomalies compared to in-situ observations.

Variable / Stat. Met.	East		Central		West	
	r	*RMSE* (mm/month)	*r*	*RMSE* (mm/month)	*r*	*RMSE* (mm/month)
Precipitation	0.59	30.72	0.62	31.89	0.46	39.10
SPI1	0.61	0.88	0.65	0.83	0.58	0.91
SPI3	0.62	0.87	0.66	0.83	0.63	0.88
SPI6	0.65	0.84	0.67	0.81	0.61	0.90
SPI9	0.71	0.77	0.69	0.79	0.62	0.88
SPI12	0.75	0.71	0.68	0.79	0.62	0.87
SPI24	0.76	0.69	0.67	0.81	0.70	0.79
Mean SPI	0.68	0.79	0.67	0.81	0.62	0.87

Table 4. Pearson correlation coefficient of TSMP ETa and ETa anomalies compared to in-situ observations.

Variable	East	Central	West
ETa/ET0	0.90	0.94	0.93
SPAEI-SPEI1	0.64	0.69	0.57
SPAEI-SPEI3	0.61	0.70	0.65
SPAEI-SPEI6	0.63	0.70	0.60
SPAEI-SPEI9	0.72	0.73	0.52
SPAEI-SPEI12	0.78	0.74	0.59
SPAEI-SPEI24	0.77	0.76	0.67
Mean SPAEI-SPEI	0.69	0.72	0.60

Table 5. Pearson correlation coefficient and RMSE of TSMP SM and SM anomalies compared to in-situ observations.

Variable / Stat. Met.	Twente network		Raam network		ISMN	
	r	*RMSE* (m^3/m^3)	r	*RMSE* (m^3/m^3)	r	*RMSE* (m^3/m^3)
SM	0.63	0.28	0.57	0.13	0.88	0.10
SSMI1	0.59	0.97	0.22	1.65	-	-
SSMI3	0.63	0.93	0.18	1.89	-	-
SSMI6	0.65	0.87	0.42	1.92	-	-
SSMI9	0.61	0.87	0.51	1.96	-	-
Mean SSMI	0.62	0.91	0.33	1.86	-	-

Table 6. Pearson correlation coefficient of TSMP WTD compared to GWL in-situ observations.

Variable	East	Southeast	Central	Southwest
WTD	-0.56	-0.38	-0.21	-0.56
	-	0.04	-	-

The statistical metrics denote that the representation of PR anomalies (i.e., SPI) is slightly better than that of the absolute values. Furthermore, the average *r* coefficient of the PR anomalies in the East (0.68) is higher than that in the Central (0.67) and Western (0.62) parts, indicating a better simulation of the dynamics. The representation of the magnitudes is better in the Eastern station as well (average *RMSE* of 0.79). On the other hand, the *r* coefficient increased in the East, and the *RMSE* reduced with the time scale. Furthermore, the best simulation in the East and the West was at a 24 month-average. However, in the central station, the best representation was obtained at a 9-month average (Table 3).

The ET indices were also compared with (PR-ETa, SPAEI) for the modeled dataset and (PR-ET0, SPEI) for the in-situ dataset. The most intense drought periods, according to the Central and Eastern stations, were 1996 and 2018. Modeled and in-situ data had a good fit for these two events at almost all the time scales (Figure 11a, c). The exceptions would be the 1996 event at a 24-month scale in the Central station (Figure 11d) and the 2018 event in the Eastern station at a 24-month scale as well (Figure 11b). Additionally, in the Eastern station, there is a strong breach between observed and modeled data in 2019 at all time scales (Figure 11a, b). As mentioned earlier, the Western station only has data available from 1999. For this station, 2018 was also the most severe drought event, followed by 2011 on the short time scale (3 and 6-month average). The event of 2003 becomes more prominent at longer time scales (9 to 24-month scale). However, according to the model data, the 2003 event was more intense than the one depicted by the in-situ data (Figure 11e, f). For the Eastern and Central stations, 2003 was also a dry period, but less prominent than 1996 and 2018 (Figure 11a, b, c, d).

There are some inconsistencies among modeled and in-situ observations. For instance, ET0 anomalies from the in-situ observations show a dry period in 2009 for the Central and Western stations. The model simulation misses this event (Figure 11c, d, e, f). Based on the SPI observations, a PR deficit was also observed by the in-situ observations this year (Figure 10c, d, e, f), indicating that the SPAEI calculated with the model dataset might be incorrect for this year.

Conversely to SPI, the statistical metrics are better for the absolute values than for the anomalies. However, the r coefficients for the anomalies are still good. ET anomalies showed a higher *r* coefficient in the Central station (0.72) and the lowest one in the Western one (0.60) (Table 4).

In contrast to PR and ET, SM anomalies were compared for a short period, constrained by in-situ data availability. Therefore, it is impossible to draw conclusions about the anomalies based on such a short period. Thus, the SSMI graphs are only referential. In contrast to PR and ET, statistic metrics were estimated at 1, 3, 6, and 9-month average. Regarding the ISMN station located in Zuid-Holland, data was available only for 11 months, therefore the SSMI was not even calculated. Despite the lack of enough in-situ data, TSMP dataset seems to represent the dynamics of SM observations. Based on the statistical metrics, the station located in Overijssel has a good *r* coefficient of 0.62, while the one located in Noord-Brabant is pretty low (0.33). The *RMSE* is also higher in the reference point of Noord-Brabant than the one of Overijssel (Table 5). The low agreement between in-situ and TSMP data anomalies in Noord-Brabant can be explained due to the existence of a gap almost at the beginning of the in-situ data, which makes the in-situ data time series shorter than the modeled data (Figure 12c, d). This adds to the already explained uncertainty at the endpoints (Section 4.4).

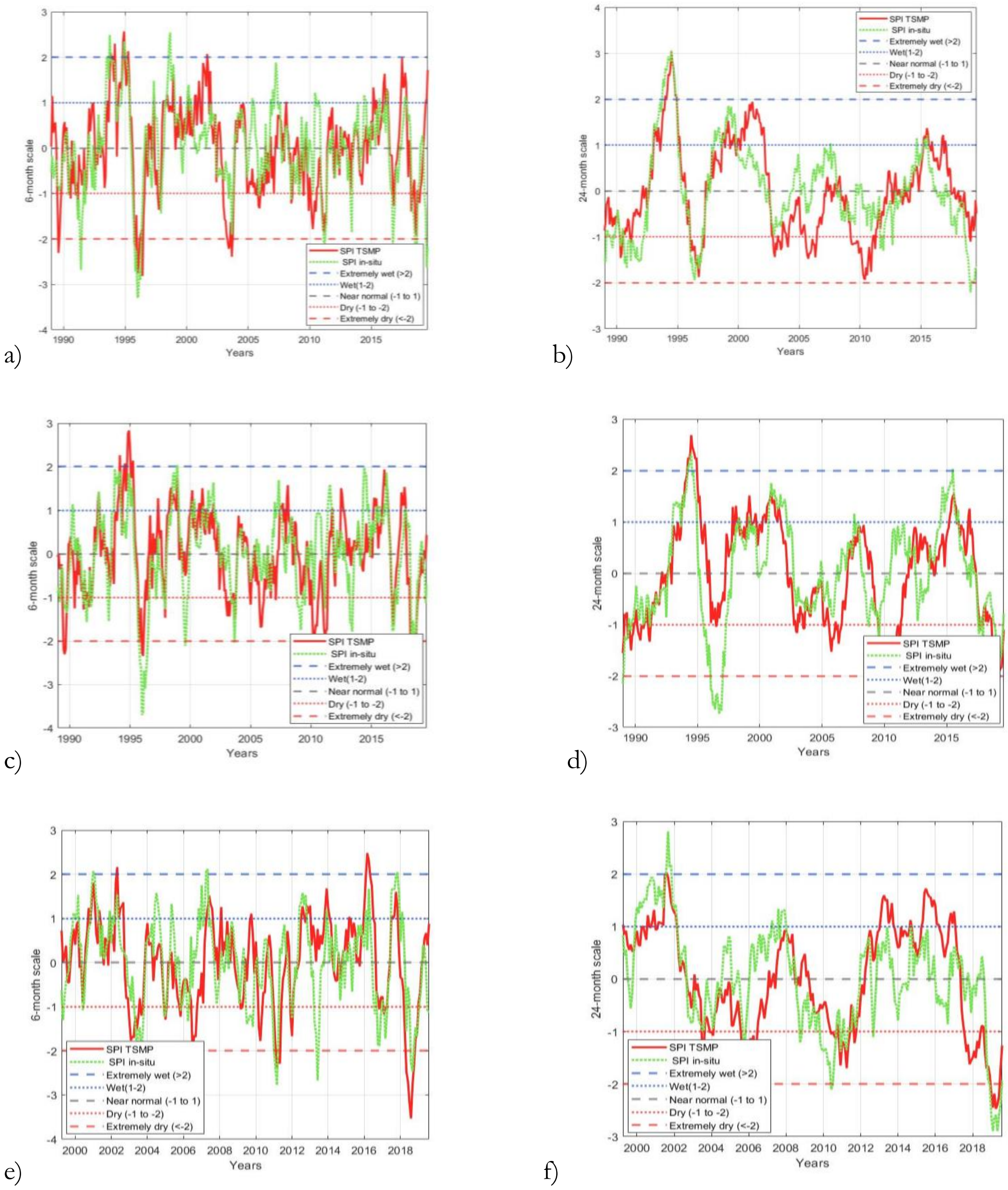

Figure 10. Comparison between short and long-term PR anomalies (SPI): (a,b) 6.891E 52.274N, Eastern Netherlands (Overijssel province), (c,d) 5.873E 52.056N, Central Netherlands (Gelderland province), (e,f) 4.979E 52.644N, Western Netherlands (Noord-Holland province).

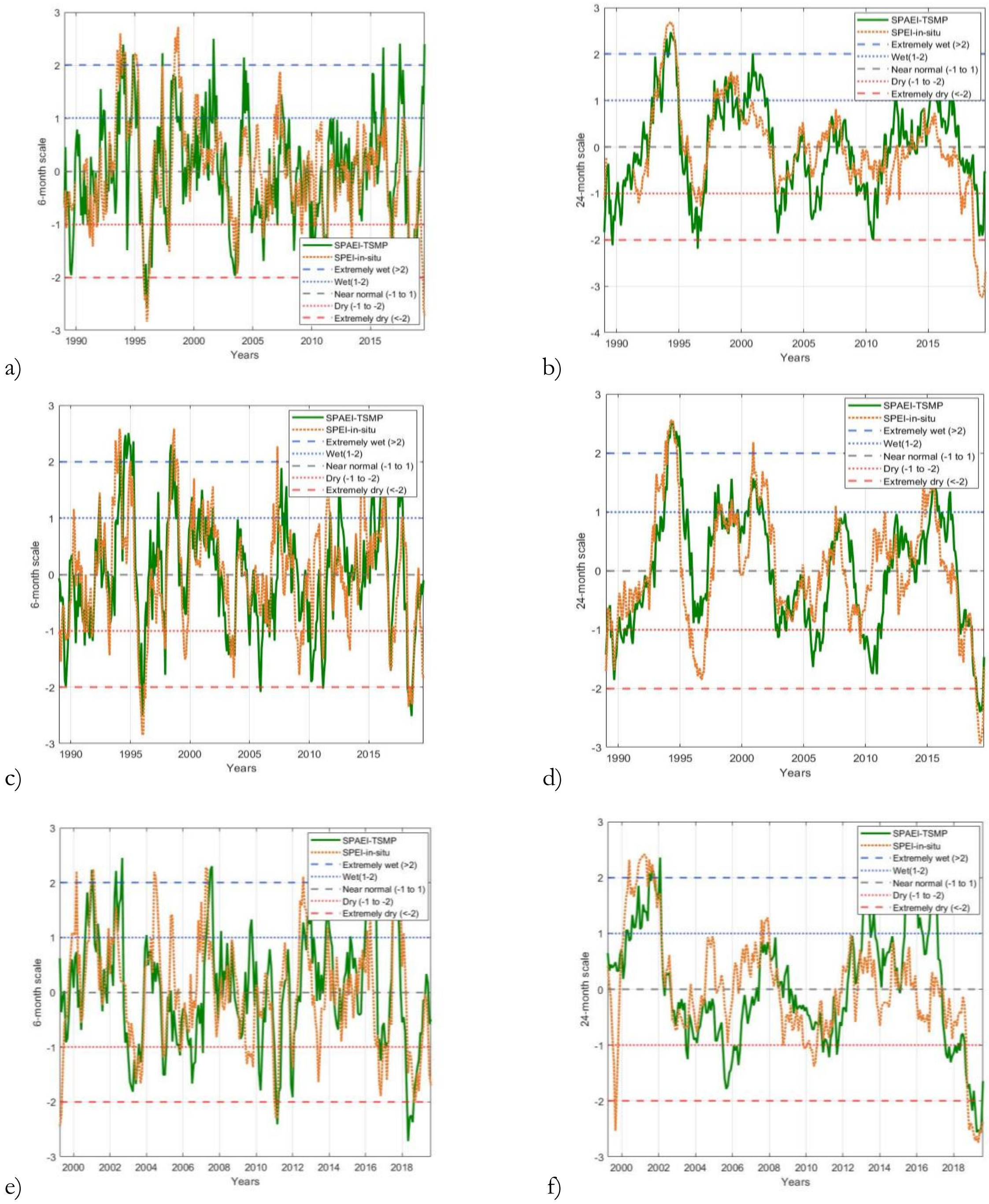

Figure 11. Comparison between short and long-term ET anomalies (SPAEI-SPEI): (a,b) 6.891E 52.274N, Eastern Netherlands (Overijssel province), (c,d) 5.873E 52.056N, Central Netherlands (Gelderland province), (e,f) 4.979E 52.644N, Western Netherlands (Noord-Holland province).

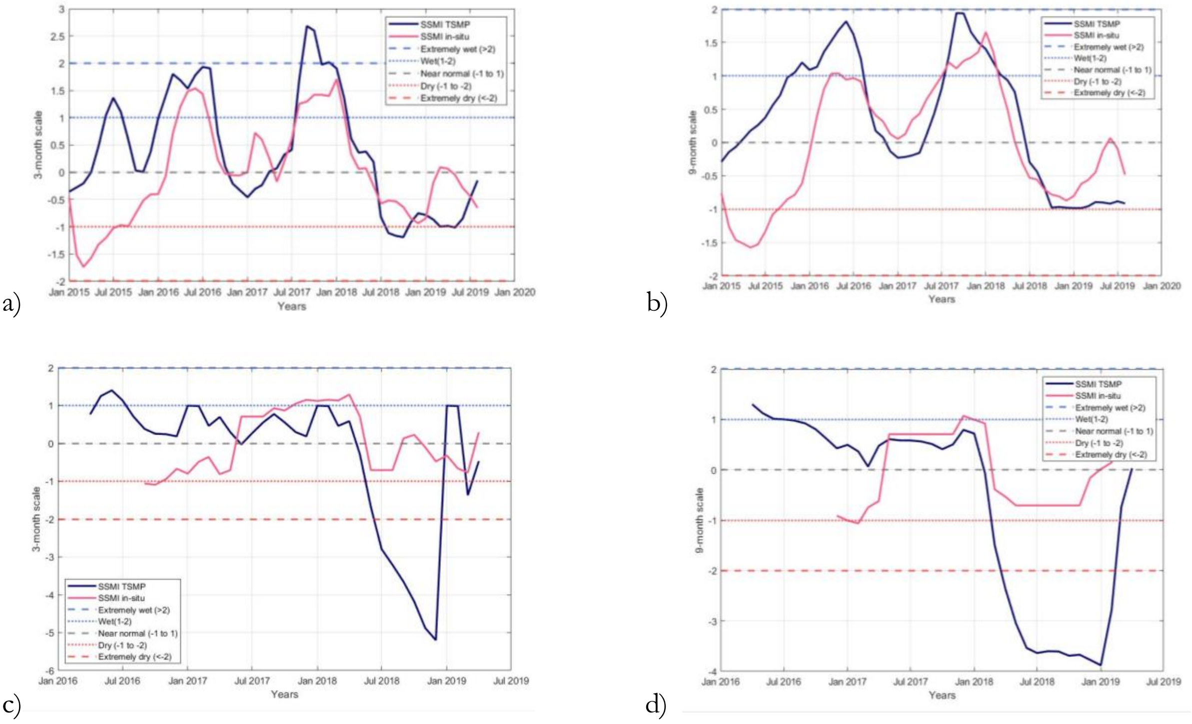

Figure 12. Comparison between short and medium-term SM anomalies (SSMI): (a,b) 6.921E 52.272N, Eastern Netherlands (Overijssel province), (c,d) 5.665E 51.710N, Southeastern Netherlands (Noord-Brabant province),

5.3. Country-scale drought assessment

5.3.1. Temporal drought indices responses

The whole country average was calculated for the SPI, SPAEI, SSMI, and STWSI based on the TSMP data. Meteorological anomalies (SPI and SPAEI) showed similar responses, while on the other hand, SM (SSMI) and hydrological anomalies (STWSI) also had a relatively closer representation. From a 6-month average, and more clearly, from a 9-month average, a delayed response is observed for some events in the SM and the TWS in the soil and the aquifer. Examples of this delayed response can be visualized in 2003 and 2011 at a 9-month average (Figure 14).

The magnitudes of the responses among different types of droughts are dissimilar. Mostly, meteorological anomalies show an enhanced dry/wet conditions than SM and hydrological anomalies. The exception would be the 2018 drought, where the hydrological, followed by the SM drought, had a higher intensity for all the time scales.

The time series indicate that there were some extremely dry periods. Some of them lasted months, while others lasted years. The propagation across the water cycle was also different, with a number of events that presented similar drought intensities for all the evaluated anomalies, while others showed milder effects for specific drought types and more intense effects for others. For instance, 2011 was a fast, extremely dry event captured at a 1, 3, and 6-month scale and propagated in almost the same intensity through the meteorological, SM, and hydrological dimensions. Another example is the 1996 event. This event lasted longer than the 2011 event and maintained extremely dry conditions, even on a 9-month scale. However, the impact of the drought was mainly on the meteorological dimension (Figures 13, 14, 15).

A particular case is 2018. This event occurred at the edge of the time series, meaning that it should be interpreted cautiously. As explained in Section 4.4, a moving average window was used in the indices calculation, meaning that at a 12-month average, the inaccuracy progressively increases from the fifth month before the end of the time series. At a 24-month average, inaccuracy progressively increases from the eleventh month. However, according to the TSMP dataset, taking out the months located at the endpoints, 2018 still was the most intense dry period, with even more dramatic effects on the soil and the aquifer.

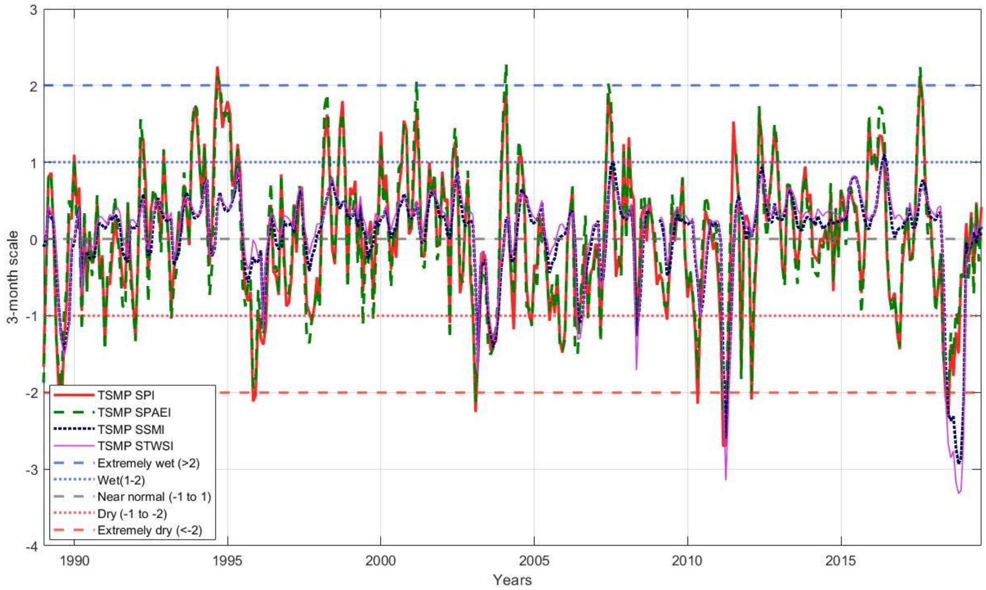

Figure 13. Average country-scale time series at a short-term response (3-month average).

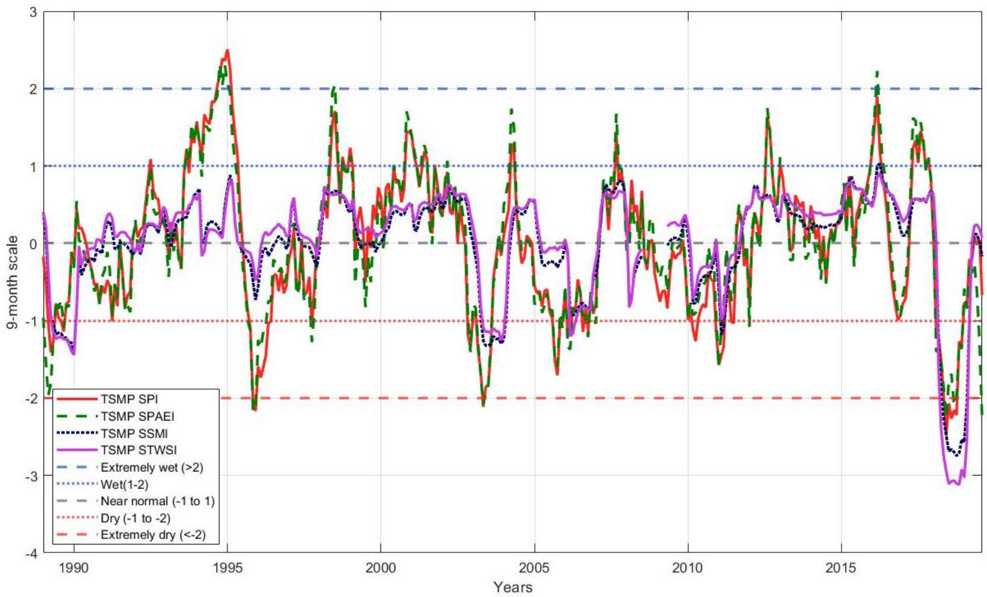

Figure 14. Average country-scale time series at a medium-term response (9-month average).

Figure 15. Average country-scale time series at a long-term response (24-month average).

5.3.2. Spatio-temporal droughts in the Netherlands

In order to observe the evolution of three selected drought events: 1996, 2003, and 2018 a 9-month average was chosen since it represents medium-term responses. According to the time series (Figure 13), these events were extremely dry in one or more dimensions (meteorological, SM, and hydrological). A series of maps were plotted for the onset, maximum dry conditions, and end of the meteorological and hydrological droughts. As mentioned, the drought of 2018 is a special case since the event took place close to the end of the time series. Hence, the results in this regard should be taken cautiously (see sections 4.4 and 5.3.1 for further details).

a) Drought 1996: In June 1995, the hydrological drought started to develop in the Northeast (NE). Slightly dry conditions presented at a 6-month average, and severely dry conditions at a 9 and 12-month average. Severely dry ET anomalies are also observed in the NE at a 6-month average. It indicates that the definition of the onset of a drought depends on the selected time scale. In July 1995, the meteorological drought started. The impact is significant in the North, especially for the ET anomalies. The maximum for both the meteorological and hydrological drought was reached in December 1995. The spatial magnitude of the meteorological drought was higher than the SM and hydrological drought. Particularly, at a 3 and 9-month scale, severely and extremely dry meteorological anomalies (almost) covered the whole country. On the other hand, SM and the hydrological drought mostly affected the NE region of the Netherlands, also reaching extremely dry conditions. When the hydrological drought ended in February 1996, severely to extremely dry conditions still persisted in the NE around Groningen and Drenthe for the SM and hydrological dimensions. At a 9 and 12-month average, the meteorological drought anomalies progressively reduced in the South. However, the NE (SPI) and East (SPAEI) remained as extremely dry areas. The end of the meteorological drought was in February 1997. Indeed, SM and TWS anomalies are mostly near-normal conditions, whereas PR and ETa anomalies are still slightly dry in the SW.

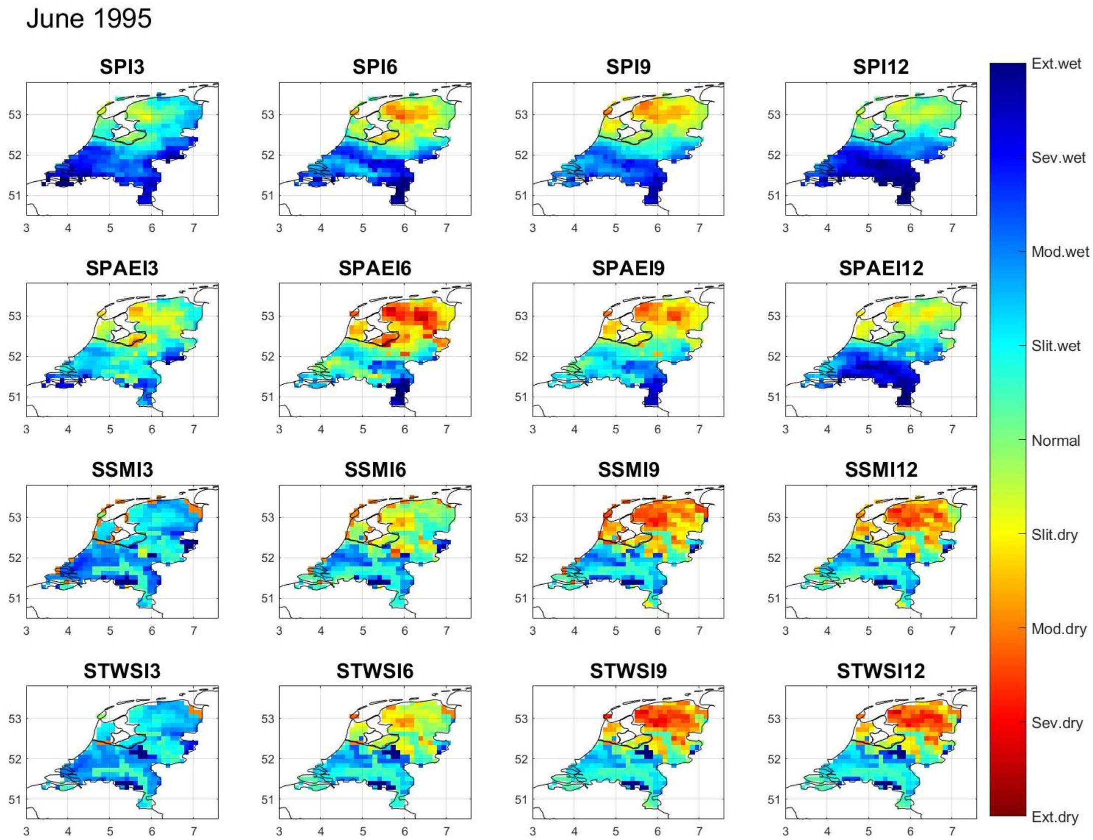
June 1995
SPI3
SPI6
SPI9
SPI12
SPAEI3
SPAEI6
SPAEI9
SPAEI12
SSMI3
SSMI6
SSMI9
SSMI12
STWSI3
STWSI6
STWSI9
STWSI12
Ext.wet
Sev.wet
Mod.wet
Slit.wet
Normal
Slit.dry
Mod.dry
Sev.dry
Ext.dry

a)

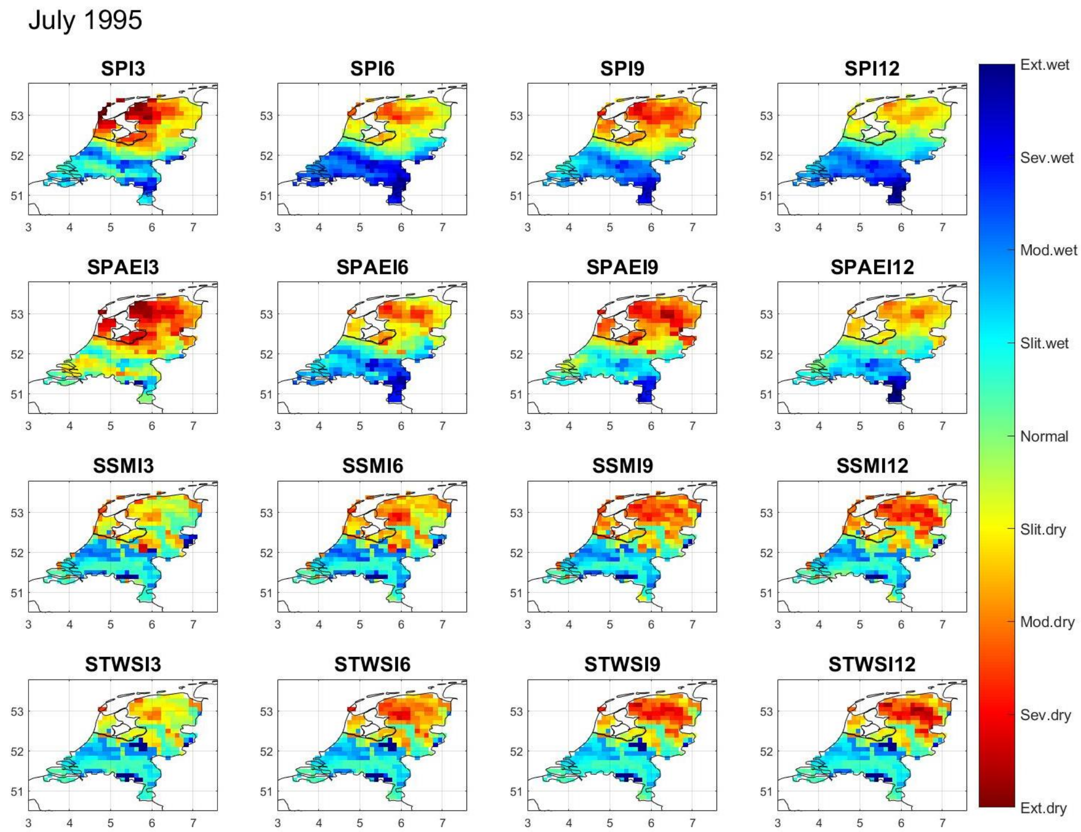
July 1995
SPI3
SPI6
SPI9
SPI12
SPAEI3
SPAEI6
SPAEI9
SPAEI12
SSMI3
SSMI6
SSMI9
SSMI12
STWSI3
STWSI6
STWSI9
STWSI12
Ext.wet
Sev.wet
Mod.wet
Slit.wet
Normal
Slit.dry
Mod.dry
Sev.dry
Ext.dry

b)

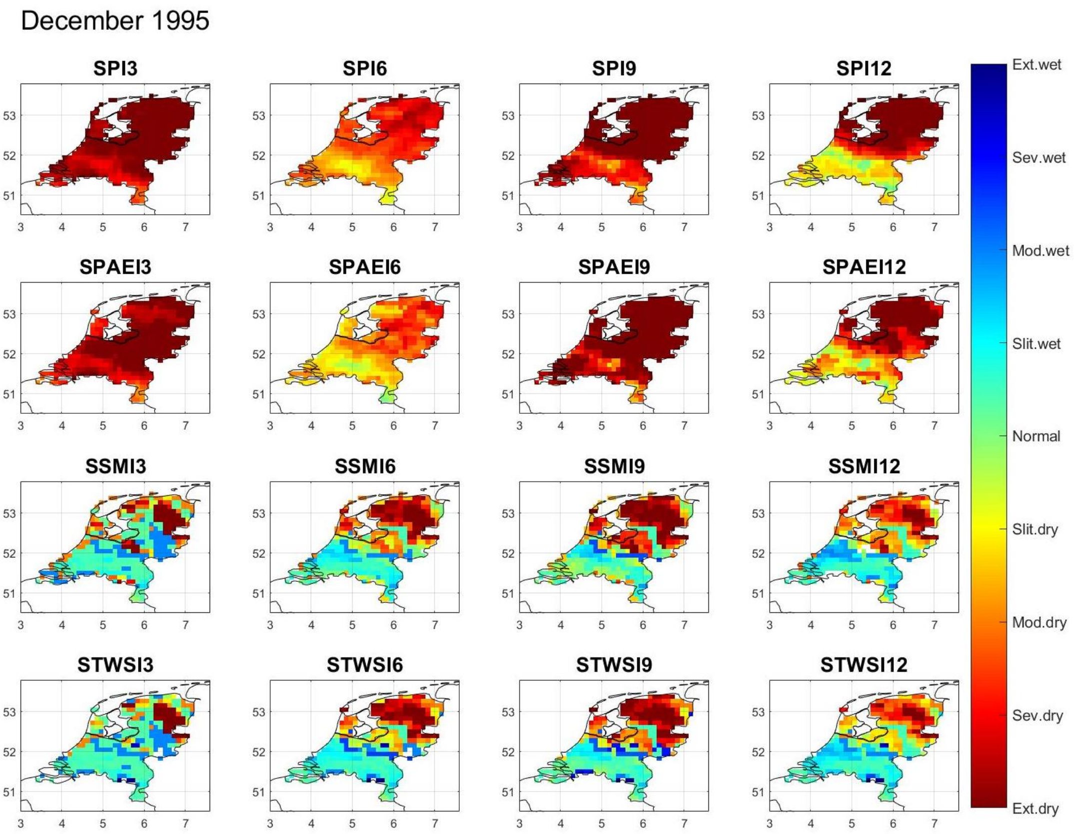
December 1995
SPI3
SPI6
SPI9
SPI12
SPAEI3
SPAEI6
SPAEI9
SPAEI12
SSMI3
SSMI6
SSMI9
SSMI12
STWSI3
STWSI6
STWSI9
STWSI12
Ext.wet
Sev.wet
Mod.wet
Slit.wet
Normal
Slit.dry
Mod.dry
Sev.dry
Ext.dry

c)

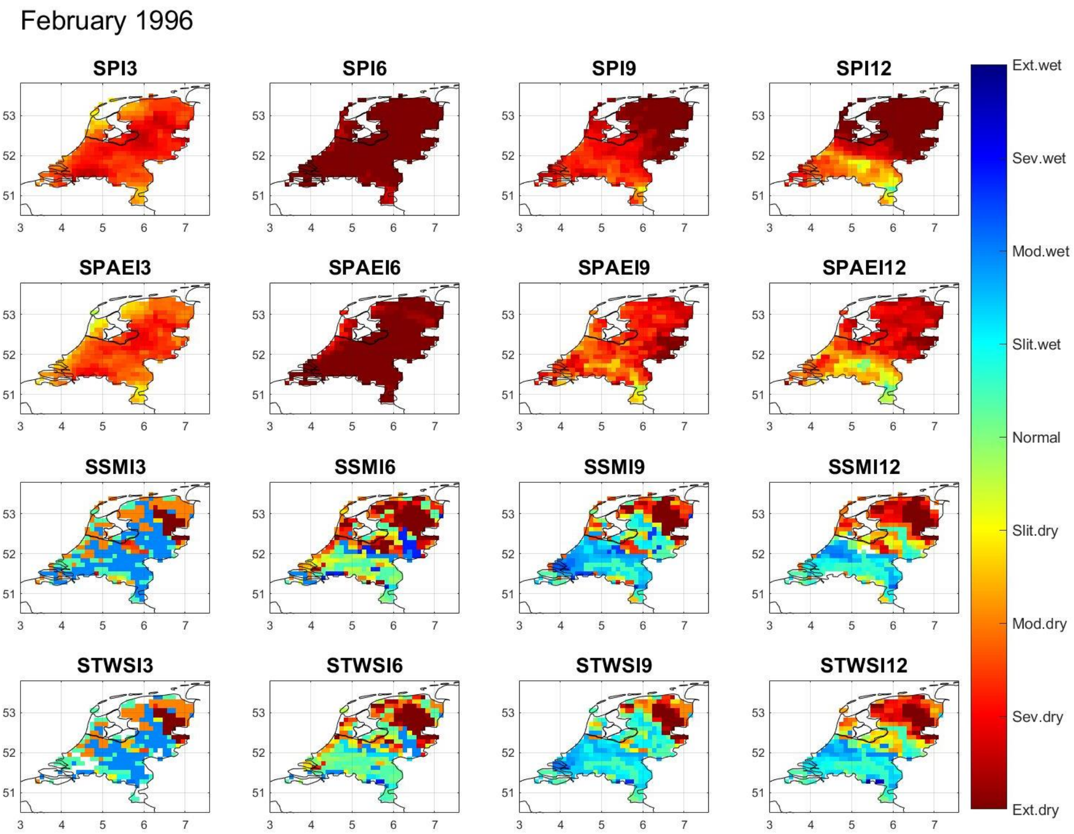
February 1996
SPI3
SPI6
SPI9
SPI12
SPAEI3
SPAEI6
SPAEI9
SPAEI12
SSMI3
SSMI6
SSMI9
SSMI12
STWSI3
STWSI6
STWSI9
STWSI12
Ext.wet
Sev.wet
Mod.wet
Slit.wet
Normal
Slit.dry
Mod.dry
Sev.dry
Ext.dry

d)

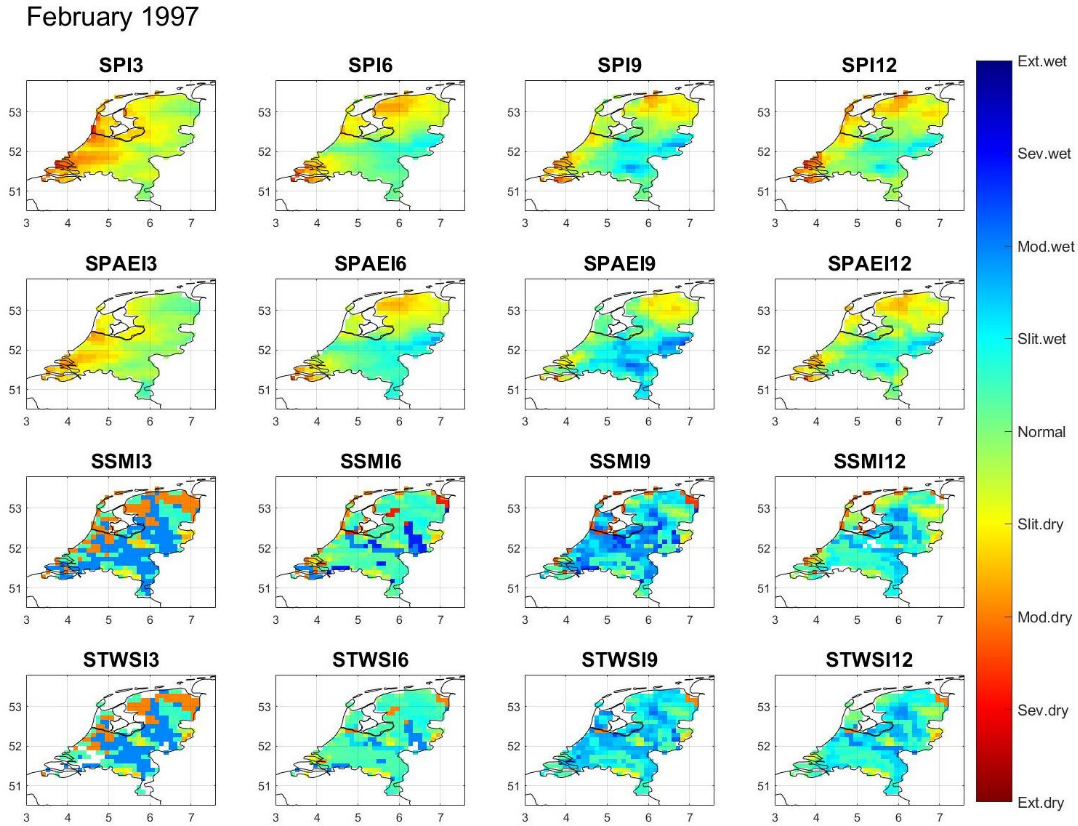

e)

Figure 16. Maps of the 1996 event (a) hydrological drought onset, (b) meteorological drought onset, (c) maximum meteorological and hydrological drought, (d) hydrological drought end, (e) meteorological drought end.

b) Drought 2003: The meteorological drought started in the NE of the country in October 2002 with slightly dry conditions in the provinces of Friesland, Groningen, and Drenthe at a 3, 6, and 9-month average. At a 12-month average, severely dry conditions are visible in the East. As the drought evolved in March 2003, severely and extremely dry anomalies covered almost the whole country in the meteorological dimension. Together with the NE, another highly affected area is observed to the SW (between Zeeland and Zuid-Holland). SPI and SPAEI showed similar patterns, but the intensity is higher for PR anomalies, for example, in the NE and SW. March 2003 was also the onset of the hydrological drought. The primarily affected areas for SM and hydrological dimensions are located in the NE and SW, as for the meteorological dimension. In May 2003, the meteorological drought reached its maximum, and the intensity was higher in the NE and SW of the country. The NE and SW were the most affected areas in the SM and hydrological dimensions as well and continued like this until December 2003, when the hydrological drought reached a peak. It is to note that the meteorological drought ended in October 2003. In February 2004, despite that based on a 9-month country scale average, the hydrological drought ended reaching >0 values, extremely dry conditions persisted in the NE and SW of the country over the SM and hydrological dimensions. Slightly higher intensity is observed for the SM drought.

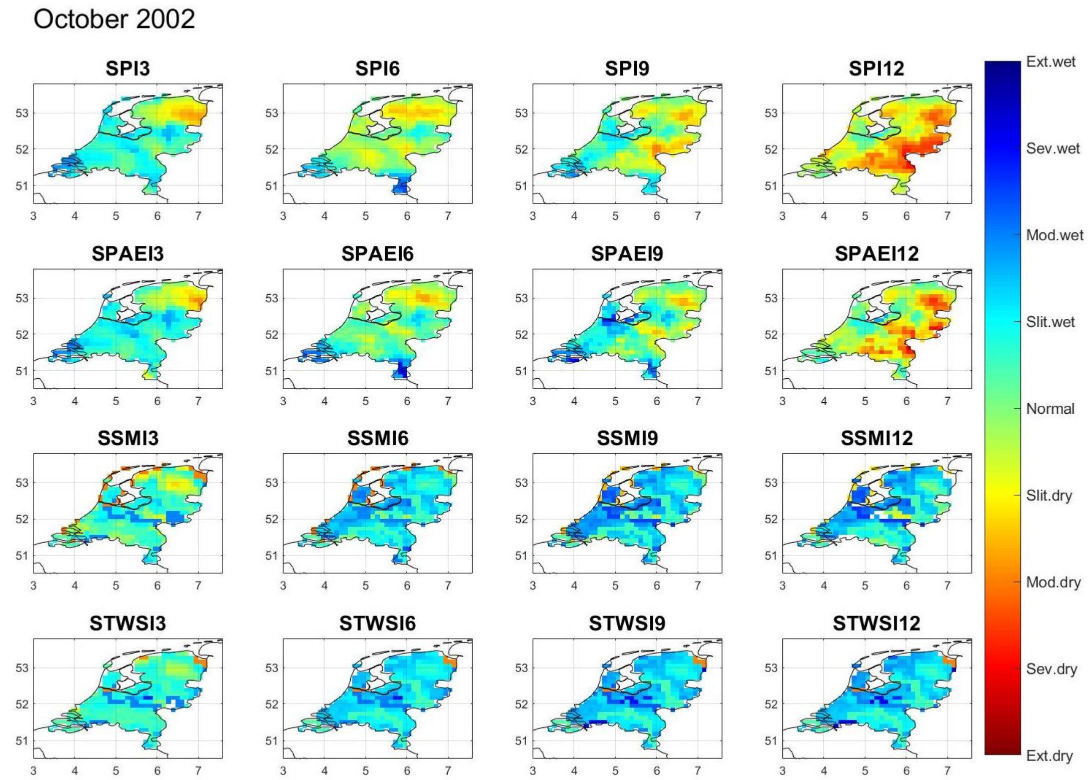

October 2002
SPI3
SPI6
SPI9
SPI12
SPAEI3
SPAEI6
SPAEI9
SPAEI12
SSMI3
SSMI6
SSMI9
SSMI12
STWSI3
STWSI6
STWSI9
STWSI12
Ext.wet
Sev.wet
Mod.wet
Slit.wet
Normal
Slit.dry
Mod.dry
Sev.dry
Ext.dry

a)

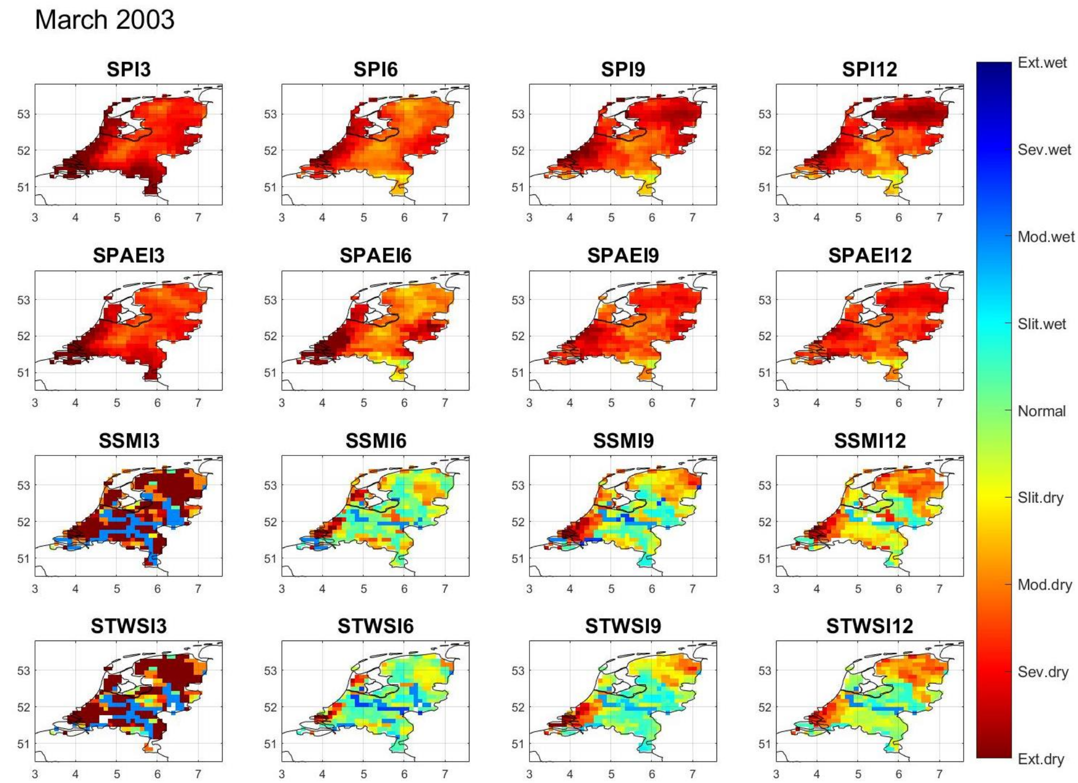

March 2003
SPI3
SPI6
SPI9
SPI12
SPAEI3
SPAEI6
SPAEI9
SPAEI12
SSMI3
SSMI6
SSMI9
SSMI12
STWSI3
STWSI6
STWSI9
STWSI12
Ext.wet
Sev.wet
Mod.wet
Slit.wet
Normal
Slit.dry
Mod.dry
Sev.dry
Ext.dry

b)

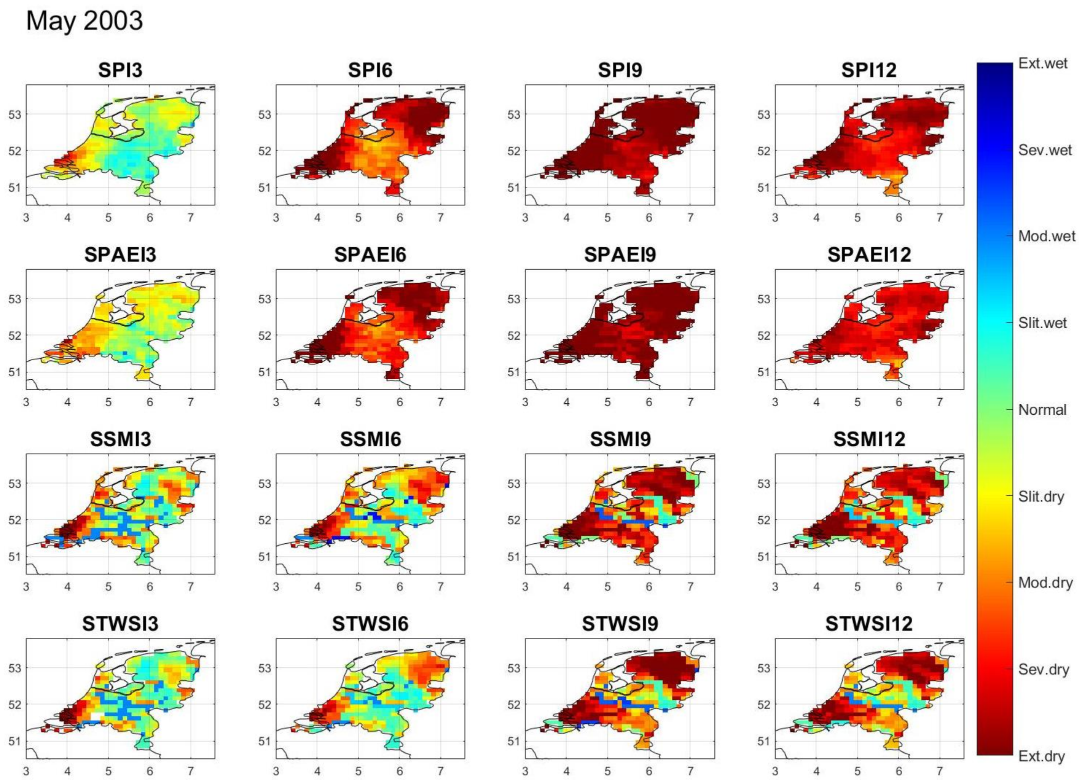
May 2003
SPI3
SPI6
SPI9
SPI12
SPAEI3
SPAEI6
SPAEI9
SPAEI12
SSMI3
SSMI6
SSMI9
SSMI12
STWSI3
STWSI6
STWSI9
STWSI12
Ext.wet
Sev.wet
Mod.wet
Slit.wet
Normal
Slit.dry
Mod.dry
Sev.dry
Ext.dry

c)

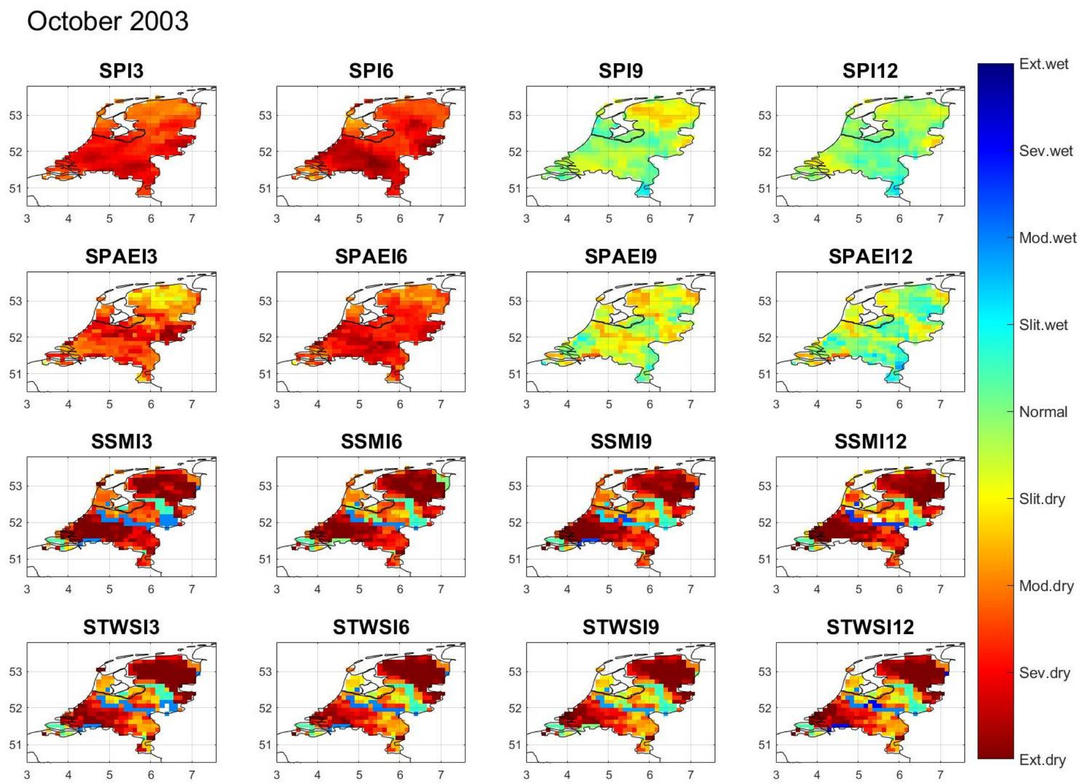
October 2003
SPI3
SPI6
SPI9
SPI12
SPAEI3
SPAEI6
SPAEI9
SPAEI12
SSMI3
SSMI6
SSMI9
SSMI12
STWSI3
STWSI6
STWSI9
STWSI12
Ext.wet
Sev.wet
Mod.wet
Slit.wet
Normal
Slit.dry
Mod.dry
Sev.dry
Ext.dry

d)

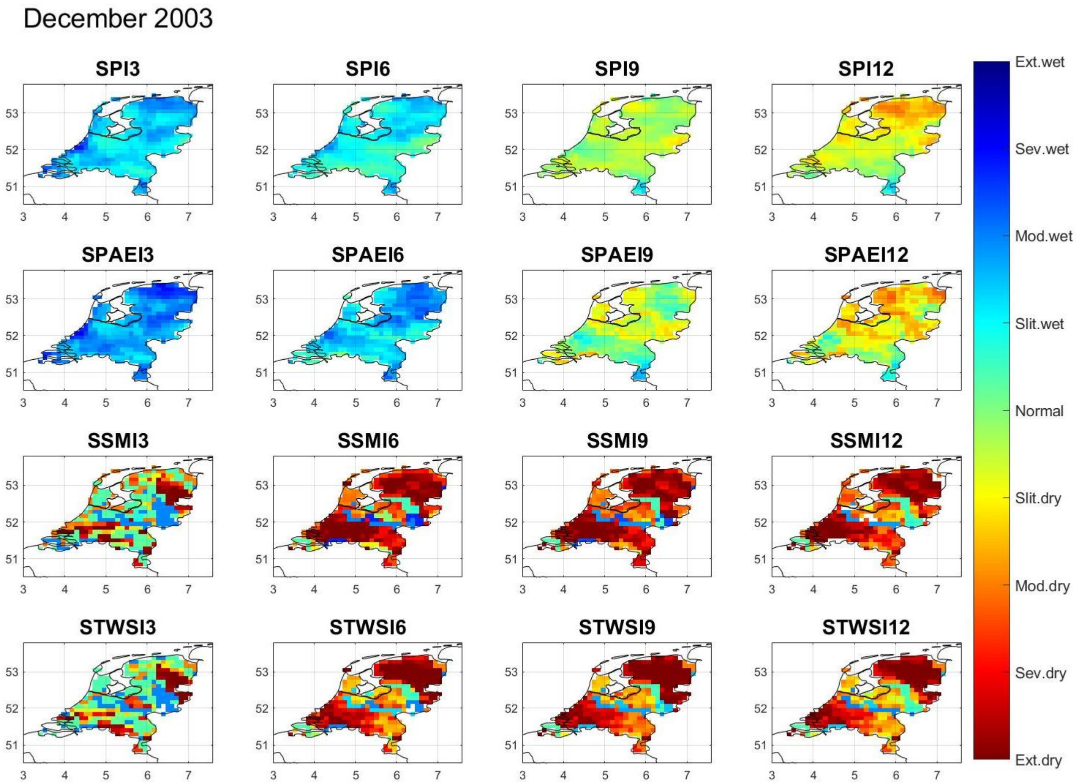

e)

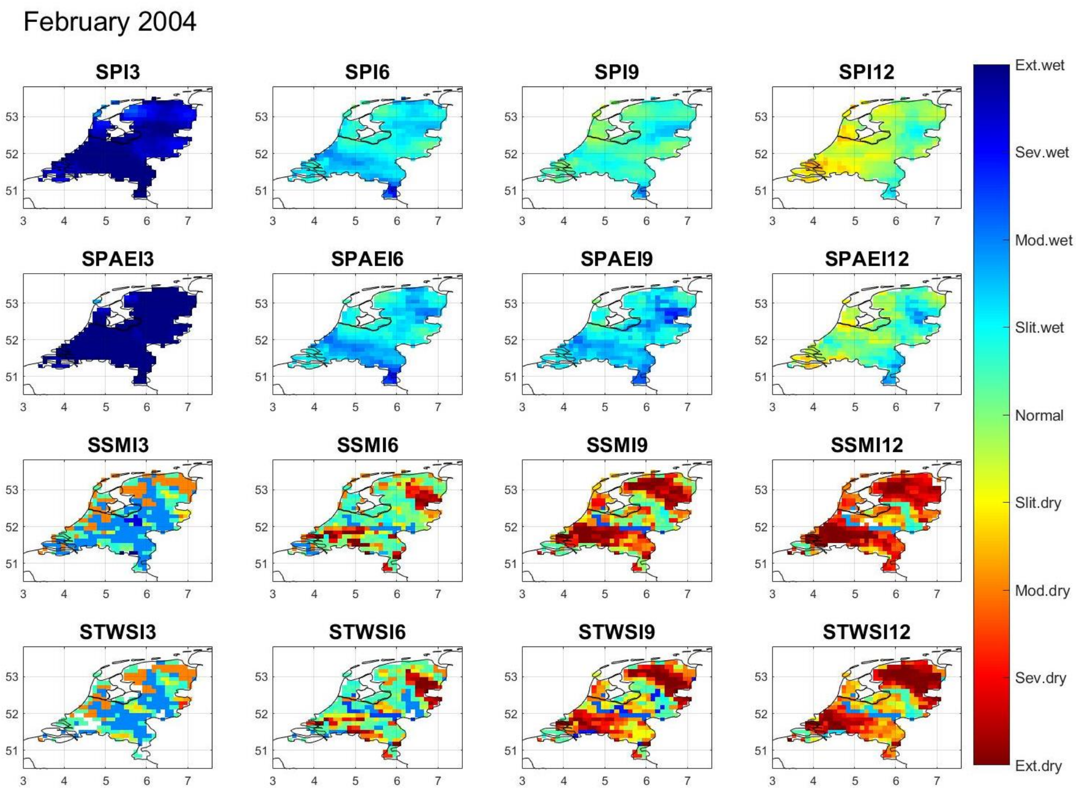

f)

Figure 17. Maps of the 2003 event (a) meteorological drought onset, (b) hydrological drought onset, (c) maximum meteorological drought, (d) meteorological drought end, (e) maximum hydrological drought, (f) hydrological drought end.

c) Drought 2018: January 2018 was the onset of the drought. Compared to the events of 1996 and 2003, the extension of the impact was the largest. The 6-month average shows that moderate dry conditions started in the inland part. March 2018 was the onset of the hydrological drought. At 9 and 12-month average, most of the country was under severely dry or dry conditions across the three dimensions, except for the Northern part. In June 2018, almost the whole country experienced severe or extreme drought during the maximum meteorological drought for all the time scales and dimensions. Compared to the previous events, the magnitude of the impact was the biggest. The exception again was the Northern part (i.e., Groningen and Drenthe), which was precisely the area where the 1996 event started and had the largest effect. In November 2018, the hydrological drought showed its maximum impact, and almost the whole country was under extremely dry conditions. March and April 2019 defined the end of the hydrological and meteorological drought, respectively. It is relevant to highlight that although based on a 9-month scale, the hydrological drought ended one month earlier than the meteorological drought, at a 12-month scale, the hydrological drought lasted longer. Thus, in April 2019, when the meteorological drought ended based on a 9-month average, at a 12-month scale, extremely dry anomalies can be visualized in the SE for the SM and TWS drought. Therefore, the definition of the onset, duration, and end of a specific type of drought depends on the selected time scale.

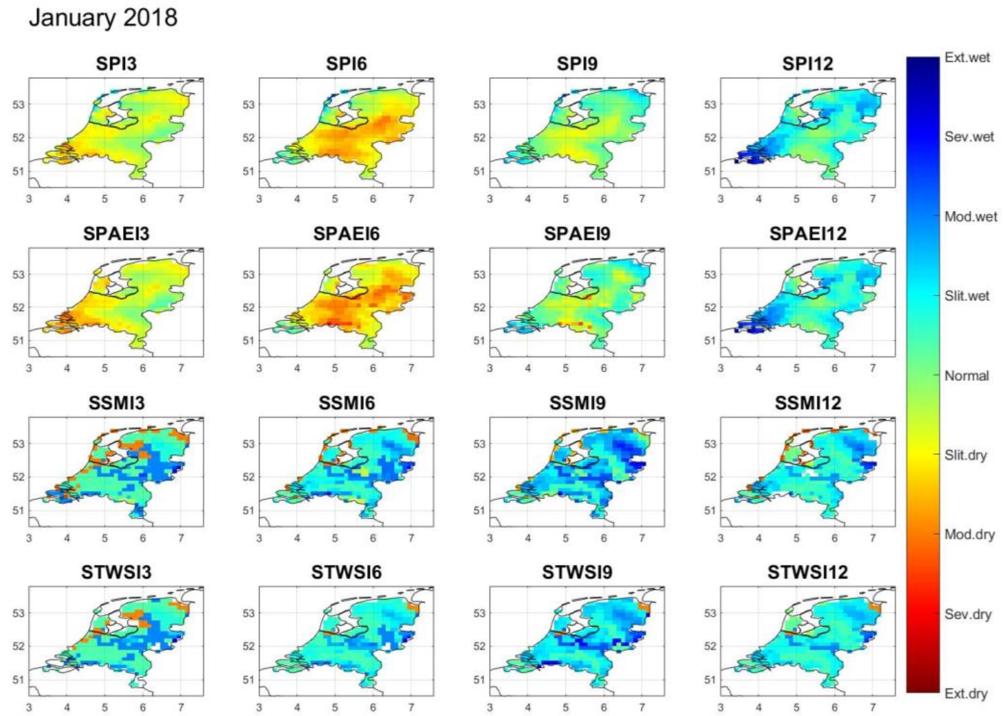

a)

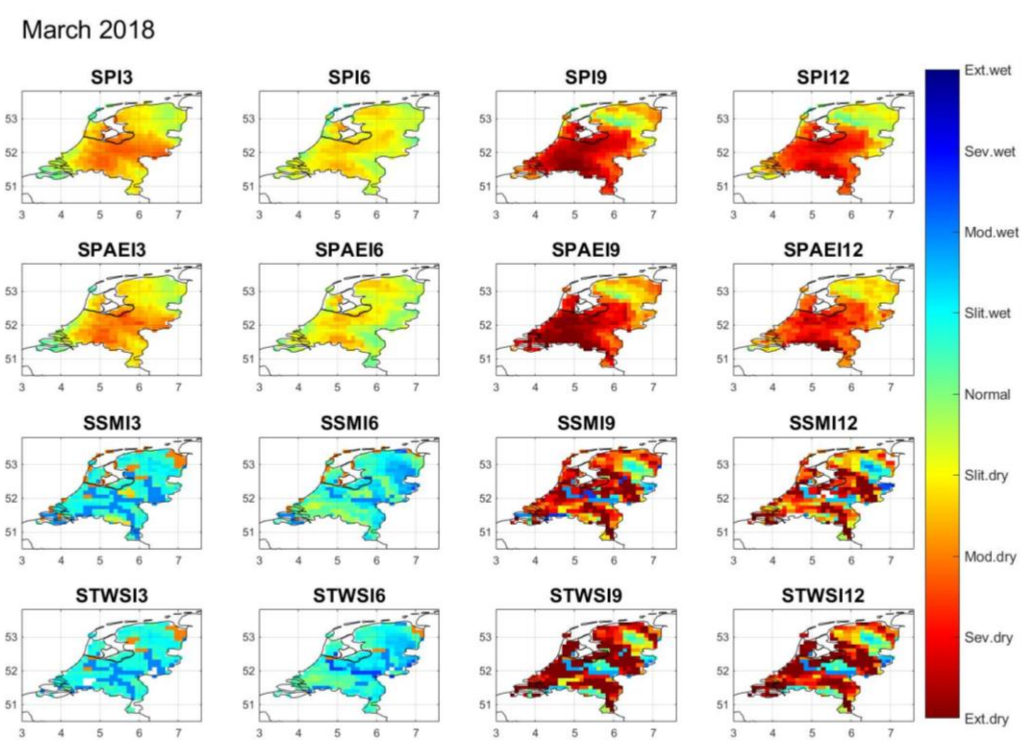
March 2018
SPI3
SPI6
SPI9
SPI12
SPAEI3
SPAEI6
SPAEI9
SPAEI12
SSMI3
SSMI6
SSMI9
SSMI12
STWSI3
STWSI6
STWSI9
STWSI12
Ext.wet
Sev.wet
Mod.wet
Slit.wet
Normal
Slit.dry
Mod.dry
Sev.dry
Ext.dry

b)

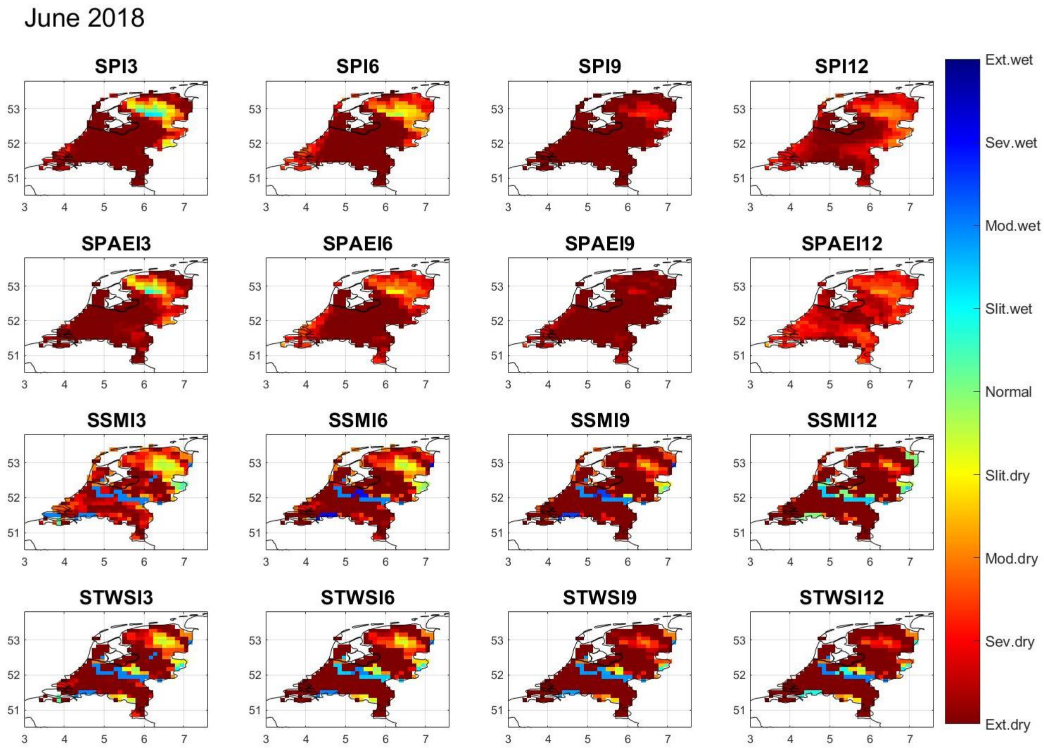
June 2018
SPI3
SPI6
SPI9
SPI12
SPAEI3
SPAEI6
SPAEI9
SPAEI12
SSMI3
SSMI6
SSMI9
SSMI12
STWSI3
STWSI6
STWSI9
STWSI12
Ext.wet
Sev.wet
Mod.wet
Slit.wet
Normal
Slit.dry
Mod.dry
Sev.dry
Ext.dry

c)

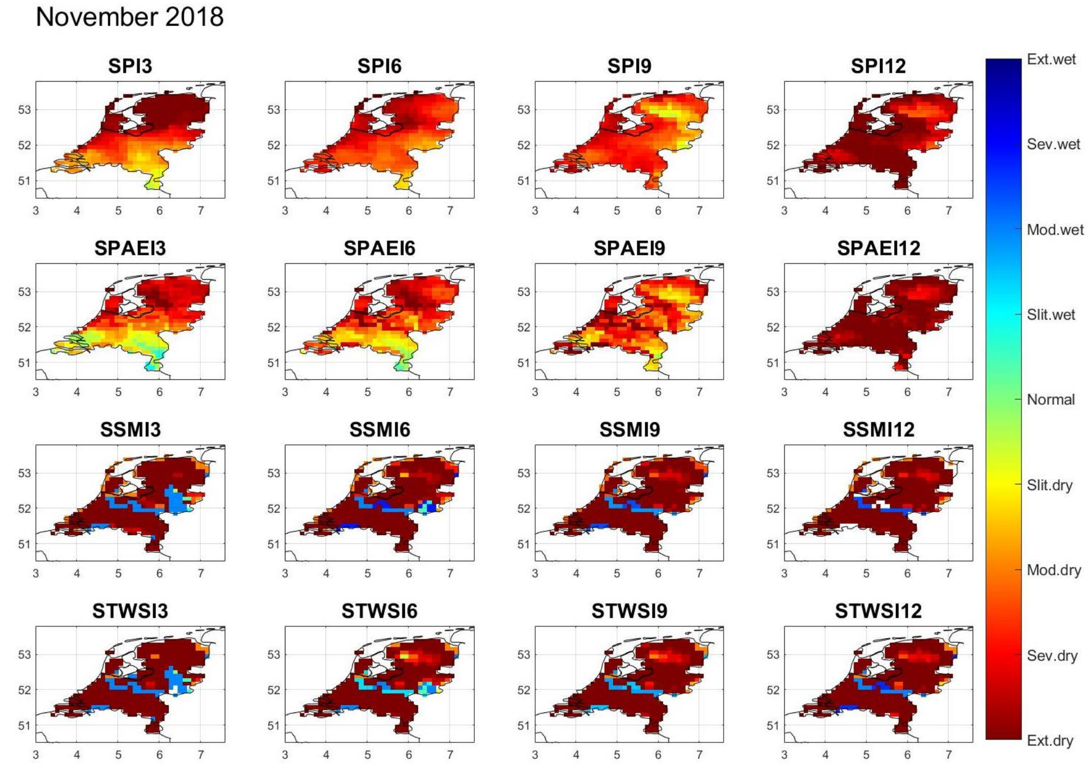
November 2018
SPI3
SPI6
SPI9
SPI12
SPAEI3
SPAEI6
SPAEI9
SPAEI12
SSMI3
SSMI6
SSMI9
SSMI12
STWSI3
STWSI6
STWSI9
STWSI12
Ext.wet
Sev.wet
Mod.wet
Slit.wet
Normal
Slit.dry
Mod.dry
Sev.dry
Ext.dry

d)

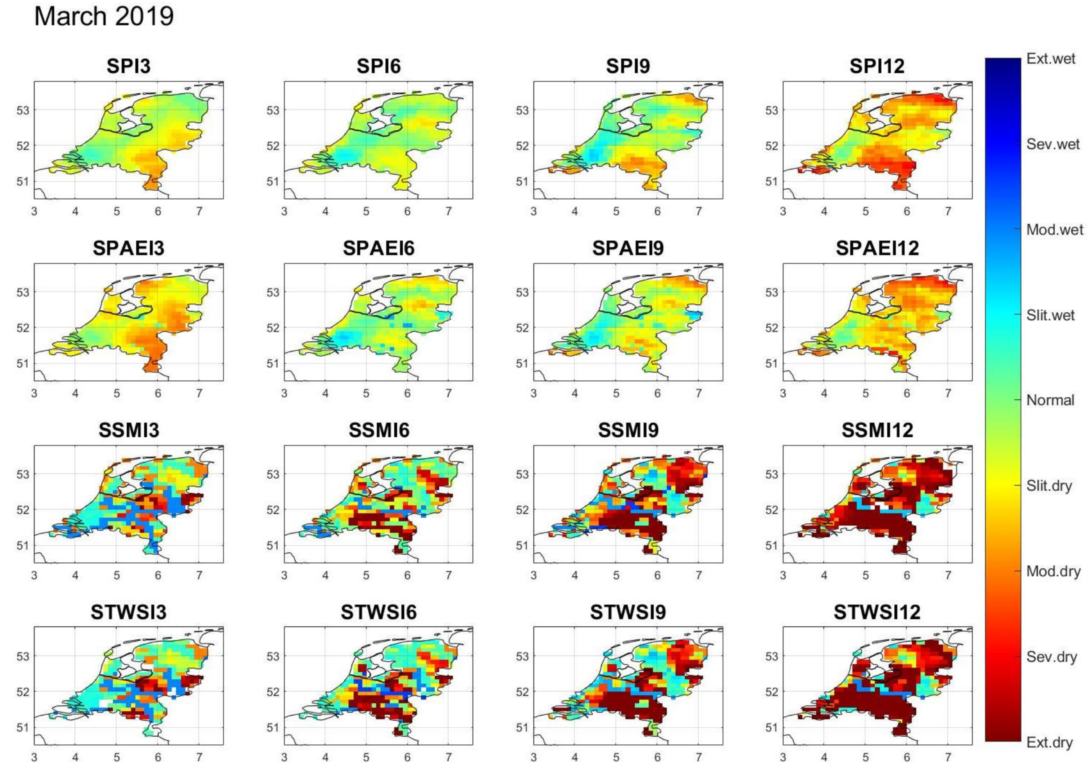
March 2019
SPI3
SPI6
SPI9
SPI12
SPAEI3
SPAEI6
SPAEI9
SPAEI12
SSMI3
SSMI6
SSMI9
SSMI12
STWSI3
STWSI6
STWSI9
STWSI12
Ext.wet
Sev.wet
Mod.wet
Slit.wet
Normal
Slit.dry
Mod.dry
Sev.dry
Ext.dry

e)

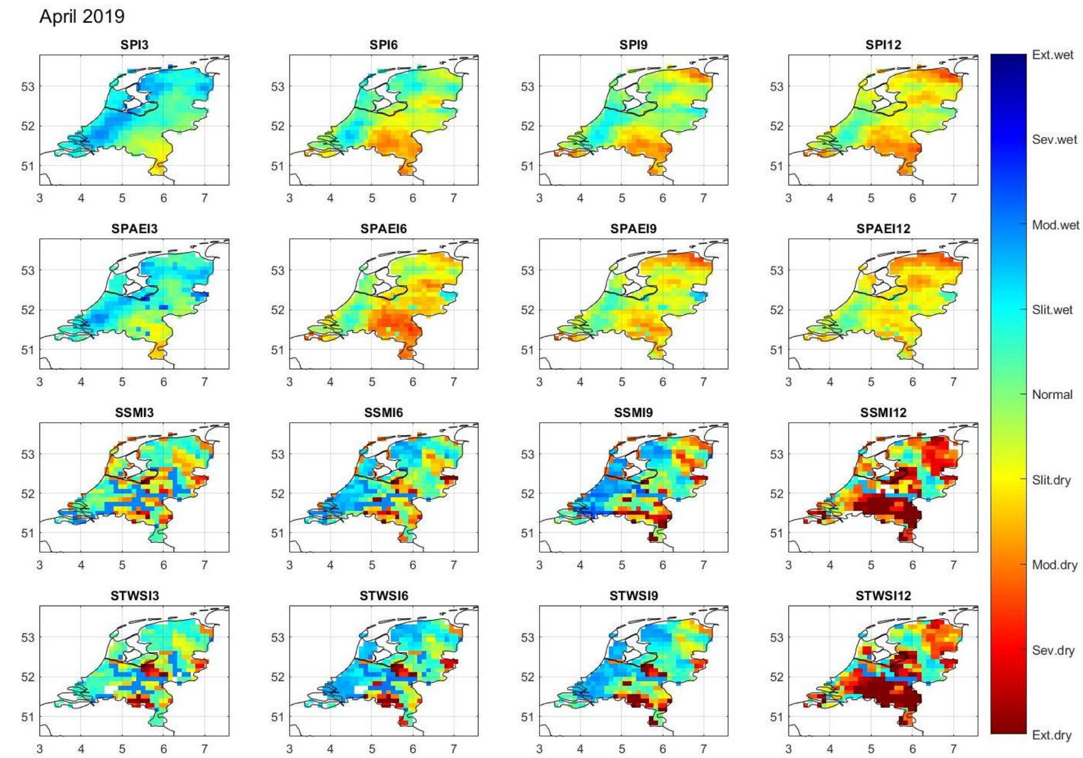

f)

Figure 18. Maps of the 2018 event (a) meteorological drought onset, (b) hydrological drought onset, (c) maximum meteorological drought, (d) maximum hydrological drought, (e) hydrological drought end, (f) meteorological drought end.

5.3.3. Probability of occurrence of extreme droughts in the Netherlands

A higher probability of occurrence of extreme droughts (≥0.04%) linked to a deficit of PR (SPI) for the whole time series (January 1st 1989 to August 31st 2019) is observed in the Northern part of the country. Medium-term (6-month average) and long-term (12-month average) extreme droughts linked to PR anomalies are more likely to occur. The frequency of occurrence of extreme droughts was remarkably higher in the North (12 to 16 episodes) for all the time scales, and in the SW and SE for the short (3-month average) and medium time scales (6-month average). On the other hand, PR-ETa deficit (SPAEI) showed a significant probability of occurrence at a 3-month average in the SW of the country. When we look at the frequency of extreme droughts, the SW had a higher number of events (12 to 16 episodes) for a short period (3 months). At other time scales, a spatial pattern for SPAEI is not evident; however, a higher occurrence of extreme droughts is observed inland than in the coastal area.

SM (SSMI) and hydrological (STWSI) droughts had a higher probability of occurrence of extreme droughts over the whole country than compared to the meteorological drought indicators. However, the impact again was stronger in the NE and SW. Based on the frequency of the events in the TWS, almost the whole NE zone experienced around 16 extreme drought events. The SM also shows a high number of extreme droughts and follows more or less the same patterns with the NE and SW as the areas with a higher frequency of extreme events.

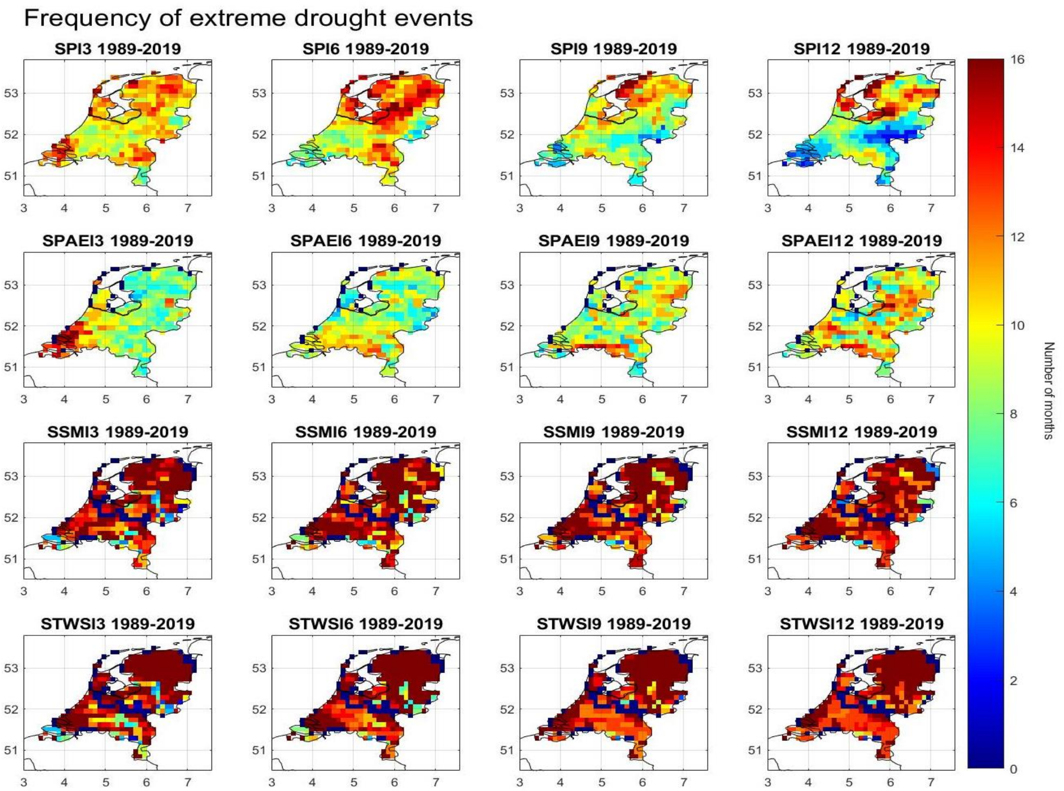

Figure 19. Frequency of extreme droughts in the Netherlands (index value <-2).

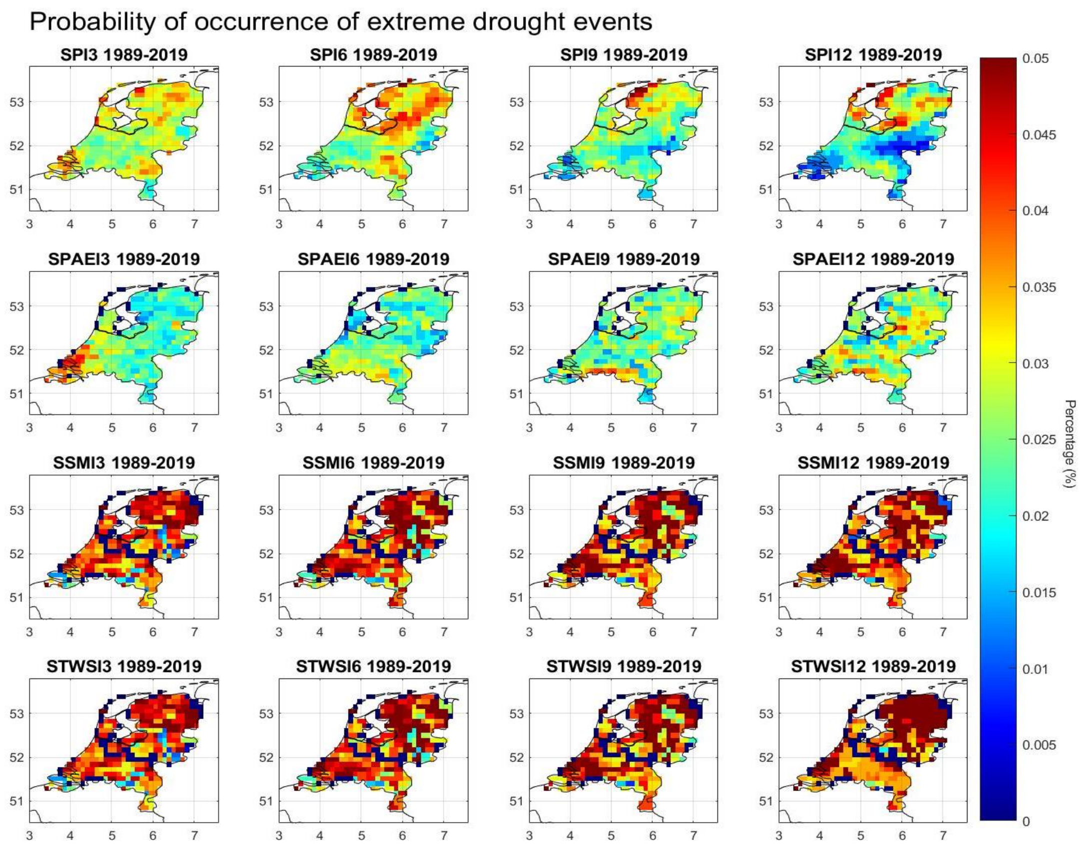

Figure 20. Probability of extreme droughts in the Netherlands (index value <-2).

6. DISCUSSION

6.1. Feasibility of using TSMP data for a country-scale drought assessment in the Netherlands

Furusho-Percot et al., (2019) indicated that TSMP data better represent the anomalies than the absolute values. Indeed, the authors validated mean T and PR anomalies from TSMP with observed gridded data (E-OBS v19) available at a 0.25° resolution. The *r* coefficients obtained after comparing these two datasets in the PRUDENCE region (the Netherlands belongs to the ME zone) ranged from 0.73 to 0.94 for mean T and from 0.62 to 0.88 for PR anomalies. This analysis was based on the period January 1st, 1996 to December 31st, 2018. On the other hand, in this thesis, PR and ETa from TSMP were assessed against the KNMI in-situ data from January 1st, 1989 to August 31st, 2019. The *r* coefficient of PR absolute values ranges from 0.46 to 0.62, and for the anomalies from 0.62 to 0.68. ET similar but not equivalent variables were also compared (i.e., ETa from TSMP and ET0 from KNMI). In this case, the *r* coefficient scores for the absolute values were higher (0.90 to 0.92).

The TWS was indirectly assessed by comparing the WTD to DINOloket in-situ measurements. From a broad perspective, Keune et al., (2016) found that the TSMP 3D simulation captures well the large-scale patterns. Accordingly, TSMP 3D model identified a shallow WTD in inundated wetlands on lowland regions such as the Netherlands and along the coastlines. This analysis focused on the European heat wave of 2003. In the present study, a point-based analysis was carried out. Our findings suggest that the representation of the dynamics performs differently across the country, with *r* coefficients ranging from 0.03 to -0.56. However, the time series plots indicate that the simulations are more or less robust. Only a comparison between the absolute values was conducted for this variable since no index was directly derived from WTD (section 5.1.4).

Hartick et al., (2021) evaluated the TSMP TWS by comparing the anomalies with GRACE observations over 2003-2011, showing a good agreement for most PRUDENCE regions, except for the Alpine region and Scandinavia. In the present thesis, SM at 5 and 10 cm depth was derived from TSMP (layers 13, 14, and 15 from the TWS). However, a limitation to assess SM data was that the short availability of in-situ measurements impeded the calculation of the SM anomalies (i.e., SSMI) in the stations from the ISMN. Nonetheless, a good *r* coefficient was obtained for the absolute values (0.57 – 0.88). Regarding the anomalies, we cannot make concluding remarks since the bias in the calculation of anomalies based on 4 or 5 years could be high. Despite that, the qualitative analysis indicates a good consistency between the in-situ and modeled data.

TSMP provides physically consistent data due to the inclusion of SM and GW dynamics in the simulation. Particularly, the analysis of extreme events such as droughts requires a closer representation of the feedbacks between the atmosphere, land surface, and subsurface compartments; and the resulting terrestrial water and energy cycle processes (Furusho-Percot et al., 2019). The validation process conducted in the Netherlands corroborated a quite acceptable performance of TSMP data, considering that the analysis consisted of comparing 12.5 km grid cells with field point stations on different locations. Therefore, a country-scale drought analysis based on TSMP may provide reliable results. A limitation of TSMP is the exclusion of human interventions in the simulation, such as water management, representing near-natural conditions (Furusho-Percot et al., 2019). However, although the Netherlands is a highly intervened area, it did not significantly diminish the performance of the dataset in the assessed points. The exception would be WTD that presented more variability between the levels of agreement with in-situ data.

6.2. Drought propagation

Drought propagation is, for example, a sequence that starts with PR deficit, followed by a decrease in SM and lower GWL. As the water deficit moves from the atmosphere to the surface and subsurface, the anomalies variations become smoother. Thus, while PR anomalies present a stronger variability, GWL does not show such extreme variations (Weijers, 2020). In most cases, the country-scale time series elaborated at 1, 3, 6, 9, 12, and 24 month-average derived from TSMP evidence the higher variability of PR and PR-ETa anomalies. Both of them show a pretty similar representation of the anomalies. On the other hand, SM and TWS present a smoother effect, but the TWS anomalies probably show slightly less variability and extremes than the SM ones. The exception is the 2018 event where the TWS dropped to extreme negative values, exceeding the meteorological and SM drought values (Figures 13, 14, 15).

Meteorological, SM, and hydrological droughts respond differently over time. After a rainfall, it takes some time for SM, and particularly GWL, to reflect positive or negative rainfall anomalies (Weijers, 2020). Figure 14 clearly shows the delay in the response of SM and the TWS (soil + aquifer). This time lag is more evident in 2003. On the other hand, the time series of Figure 14 has some apparent inconsistencies that should be interpreted cautiously. For example, the onset of the hydrological drought of 1996 was registered in June 1995 (the first month the index started to register negative values), while the onset of the meteorological drought was in July 1995. By looking at shorter time scales, we found that the meteorological drought is already visible (e.g., 6-month average), albeit, at a 9-month average, the development of the meteorological drought based on PR is barely emerging. The same was observed in the 2018 drought. The hydrological drought ended in March 2019, while the meteorological drought in April 2019. Nonetheless, by looking, in this case, at longer time scales, we found that at a 12-month average, an extreme drought persisted in the surface and subsurface (Section 5.3.2).

On the spatial scale, the time lag is also visible, and the effect over the country depends on which areas were exposed for a longer time to extreme meteorological anomalies. For instance, over the 2018 drought event, the Southern and Eastern sides were highly affected. In April 2019, when the meteorological drought ended, the SM, and with a slightly higher emphasis, the TWS still had some extremely dry areas in the South and East of the country (Figure 18f).

6.3. Response of droughts to physical processes

Based on the TSMP derived results, the drought of 1996 mostly affected the Northern and Southwestern Netherlands with higher PR and PR–ETa deficit rates. In comparison, the highest negative anomalies in SM and TWS were mainly confined to the Northeastern area (Figure 16c). The 2003 event showed two consistently impacted regions over the four analyzed water cycle anomalies: the NE and SW (Figure 17). Despite the more dynamic patterns that are observed in 2018, two highly affected areas for the meteorological, SM, and hydrological droughts were the Southern and inland regions of the Netherlands (Figure 18).

According to our observations, in these three events, PR negative anomalies associated with higher PR–ETa rates led to the droughts of 1996, 2003, and 2018. In order to examine the patterns, two stations were compared for each event. The first station represents an area with strong negative anomalies, while the other represents a slightly affected area or affected for a short period. The selected stations are presented in Table 7.

Based on the TSMP dataset, in December 1995, PR negative anomalies reached their maximum. The Northern (station 48) was the most affected area, whereas the Southeastern (station 7) responded later to the PR anomalies (Figure 19). According to KNMI measurements, despite both stations experienced an extreme drought situation (<-2), the North faced even drier anomalies and for a longer time. For instance, at a 9-month average, in the SE, the drought lasted 15 months (June 1995 – October 1996), but in the North, the drought lasted 18 months (August 1995 – February 1997). Moreover, after the drought period, a wet period followed where the SE became extremely wet, while the North presented only moderately wet conditions. Consequently, TSMP did not provide an exact picture of the onset of the phenomenon, neither did it identify an earlier onset of the drought in the SE than the Northern part and missed that the SE also faced a similar impact compared to the North. However, it was more consistent at defining a longer duration in the North and the slightly higher impact over this area than in the SE. It also captured well an earlier end of the drought in the SE, and a shift of this area to wetter conditions can also be observed.

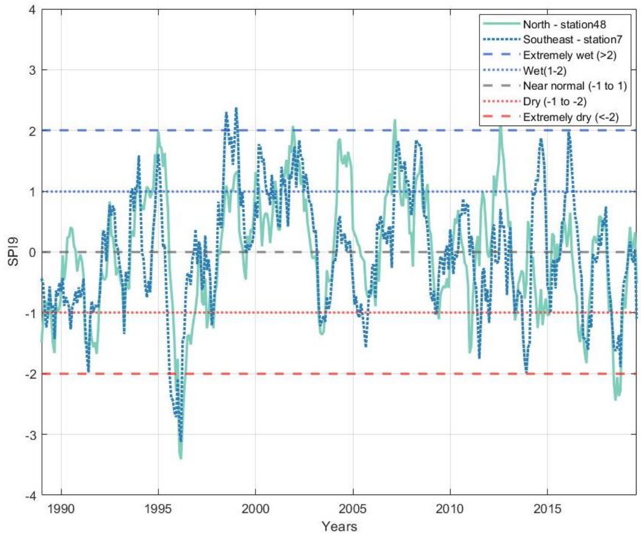

Figure 21. Comparison of PR anomalies at a 9-month average between KNMI stations 48 (North) and 7 (SE).

In the event of 2003, the NE (station 40) was compared to the SE (station 7). Based on TSMP dataset, the SE was also affected in this event, but the intensity and the duration were lower than the NE (Figure 17). On the other hand, KNMI PR anomalies show that this drought was not an extreme one (at least at these locations), and the two points registered from moderate to severe dry conditions (Figure 22). However, KNMI PR anomalies confirm that the duration of the drought was longer in the NE than in the SW. For example, at a 9-month average, the event lasted 16 months in the NE (July 2002 – November 2003), whereas in the SE, the drought lasted 11 months (March 2003 – February 2004). Therefore, TSMP dataset overestimated the intensity of the event in the NE but was more accurate at defining a longer duration in this region than in the SE.

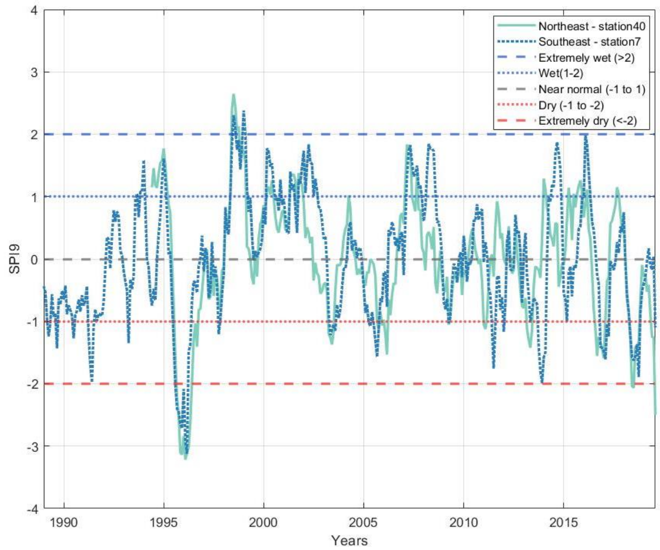

Figure 22. Comparison of PR anomalies at a 9-month average between KNMI stations 40 (NE) and 7 (SE).

TSMP derived maps show that the drought of 2018 was more dynamic, starting mainly in the central part of the country and then extending to the inland part. Later on, at the maximum peak of the meteorological drought, almost the entire country suffered extremely dry conditions, while the NE remained mostly under moderate or severe drought. By the end of the meteorological drought, moderately dry conditions still remained on the Eastern part (Figure 18). Based on the KNMI stations, the Central (station 20) and the Northeastern stations (station 40) experienced almost a similar drought intensity (Figure 23). However, at a shorter time scale (3-month average), it was slightly stronger in the central part. Regarding the duration at a 9-month scale, in the NE, meteorological drought started in February 2018, while in the Central part started in March 2018. A small recovery can be observed in the central part before dropping again, indicating that dry conditions still persisted. Nonetheless, due to the moving average, the interpretation of the endpoints should be made cautiously (see Section 4.4). TSMP data seems to be correct about the duration of the phenomena. However, the intensity of the event in contrast to the reference data is probably overestimated in the Central area and underestimated in the Northeastern area.

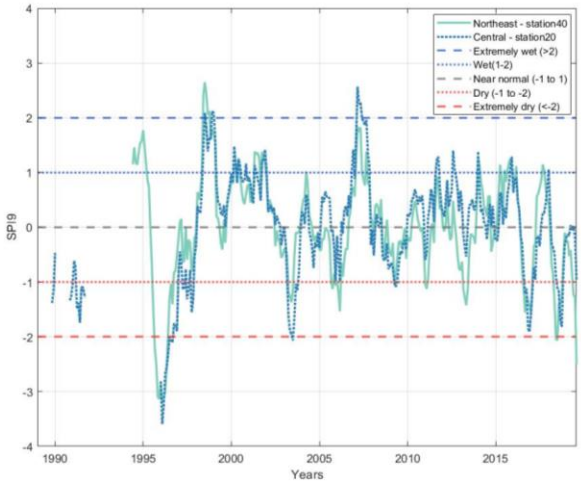

Figure 23. Comparison of PR anomalies at a 9-month average between KNMI stations 40 (NE) and 20 (Central).

Taking into account the three drought events, TSMP captured well the duration of the phenomena, such as in the droughts of 1996 and 2003. The dynamics were better represented in the 1996 event than compared to the others. Regarding the intensities, there is an inherent uncertainty, as previously discussed in the events of 2003 and 2018.

In contrast to PR, no KNMI ETa measurements exist. However, PR–ETa anomalies replicate the PR anomalies very closely. Indeed, some slight differences exist among meteorological anomalies, probably these slight differences are related to land use and soil texture. Nonetheless, based on the observations, it is impossible to define to what extent these variables influence the PR–ETa anomalies. Concerning the 2018 drought, there is an existing study from Philip et al. (2020), who pointed out that the PR shortfall calculated in the Netherlands from PR–ET0 was higher in the Southern and Eastern regions. This study corroborates the patterns observed on TSMP drought maps (Figure 16), lasting longer in the Southern and Eastern parts of the country.

According to TSMP anomalies, SM drought can be primarily explained by less available water derived from PR-ETa. The longer the period that an area was under meteorological water stress, the higher the impact on the SM. At the same time, the effect of soil texture, based on the soil type obtained from the Dutch Soil Information System (BIS-Nederland), is mainly visible in the events of 1996 and 2018. In December 1995, when the hydrological drought reached a peak, the extremely dry area moved to the NE closer to the border with Germany (Figure 16c). Sandy soils are predominant in this area, characterized for having a poor water holding capacity (Figure 3b). In contrast, the parts of Friesland and Groningen that have peat, light clay, and light loam soils with medium to high water holding capacity seem to be slightly less affected (Figure 16c). In 2018, the zone located in the inland part of the Netherlands remained the most affected (Figure 18), coinciding with sandy soils (in the SE and Central-Eastern parts) and their lower water holding capacity. Buitink et al., (2020) stated that a strong decrease in PR in June and July of 2018 led to significant negative SM anomalies, mainly in the Eastern part of the Netherlands.

The maps also reveal a connection between TWS anomalies and the recharge (PR-ETa anomalies). Furthermore, it is observed that despite the impact of the GW depth is not very well reflected, it probably played a most relevant role in the 2018 event. Deeper GWL characterizes the Eastern part of the country, and the drought in that year was more severe in this region in the hydrological dimension (Figure 17, 18).

In consequence, TSMP did not provide an exact picture of the onset and end of the phenomenon, but it was more consistent at defining some patterns (mainly in the SM and hydrological domains) and duration. At the same time, PR anomalies were either under and overestimated, for instance, in the 2003 and 2018 events. However, the model has a good correspondence with other physical characteristics such as soil texture and GWL, indicating that the model is appropriate for a country-scale drought monitoring.

6.4. Critical areas to droughts

The probability of occurrence of extreme droughts concerning PR anomalies was assessed in comparison to selected KNMI stations located in or nearby the areas of interest. The observations indicate that the SW (station 22), the North (station 48) in the coastline of the Ijsselmeer, and a NE strip (station 40) show a higher probability of occurrence at different time scales (Figure 20). A higher probability is mainly in the North and NE. Conversely, the Central (station 20) and Southeastern (station 7) regions show a lower probability (Figure 20).

Table 7. KNMI stations used in the interpretation of physical processes and identification of critical areas at a 9-month average. ID number of station corresponds to the NetCDF index of the data file.

KNMI station	Location	Latitude	Longitude	Frequency	Probability
7	Southeast	50.906	5.762	8	0.022
20	Center	51.97	4.926	10	0.033
22	Southwest	51.226	3.861	13	0.043
40	Northeast	52.75	6.574	12	0.040
48	North	53.224	5.752	10	0.027

Taking a 9-month average as a reference, the KNMI stations reveal the highest probability of extreme droughts in the SW (0.043), followed by the NE (0.040) (Table 7). On the other hand, TSMP dataset indicates that the SW is a critical area to meteorological flash droughts since the impact is observed at a 3-month scale (Figure 20). However, according to Table 7, the higher probability of occurrence of extreme droughts over the SW extends to longer time scales (i.e., 9 months). The in-situ observation in the NE agree with TSMP dataset. The North shows the second lowest probability of drought (0.027) according to KNMI observations. This finding contradicts TSMP derived results in this area since it is presented as one of the most affected areas. Conversely, TSMP findings in the Central (0.033) and Southeastern (0.022) areas are more consistent with in-situ observations. Consequently, except for the Northern part, the TSMP model provided satisfactory results identifying the most critical areas.

Concerning PR shortfall (PR–ETa), the higher probability of extreme droughts in the SW seems a response to the PR negative anomalies. On the other hand, the negative anomalies observed in the Southern part (Figure 19, 20) might reflect the overall balance of increasing T and radiation in the inland region, with no PR positive trend reported by Philip et al., (2020). The South is also characterized by sandy soils, which are drier and enhance the warming effect (Furusho-Percot et al., 2019; Haarsma et al., 2009).

The higher probability of extreme negative SM anomalies seems a response to extreme PR negative anomalies, and it is in agreement with the KNMI PR extreme negative anomalies with the SW and NE as the most affected areas (Figure 19, 20). The role of the soil texture (Figure 3b) is probably less relevant since soil types with low (sandy), medium (loam), and high (peat) water holding capacity are all experiencing the relatively higher extreme drought frequency (Figure 3b).

Finally, the TWS extreme anomalies may respond to recharge anomalies (PR-ETa) in the NE and SW and the deeper GWL in the NE.

7. CONCLUSIONS

Studies on a continental scale in Europe reveal a good performance of TSMP, except for the Alpine region and Scandinavia (Furusho-Percot et al., 2019; Hartick et al., 2021; Keune et al., 2016). In the Netherlands, the assessed TSMP variables (PR, ETa, SM, and WTD) obtained an acceptable *r* coefficient and/or qualitative representation compared to the in-situ stations. However, there are some clear under and overestimations of some water cycle variables. In contrast to other variables, WTD had a more diverse behavior concerning the levels of agreement with in-situ data. Although the *r* coefficients are moderate to low, the qualitative analysis suggests that the wet and dry periods are mostly well captured. The performance of the TSMP dataset is quite robust, considering that in-situ points were compared with 12.5 km pixels and that the model simulates near-normal conditions, whereas the Netherlands is a highly intervened area (section 6.1).

Regarding drought propagation, there is a clear distinction between meteorological from one side and SM and hydrological drought from the other side. Based on TSMP, meteorological drought, including PR and ETa anomalies, show higher variability and intensity in their response. On the contrary, SM and TWS anomalies present a smooth response and a lower intensity. It is difficult to conclude if the TWS drought anomalies are smoother and have a lower intensity than SM. An exception is 2018, when extreme negative values were registered for TWS, its intensity was higher than SM and meteorological droughts. Considering that it happens at the end of the time series, it could be a result of the inaccuracies derived from the moving average, which particularly affects the endpoints of a time series. However, more researches into this aspect would be needed. Concerning the time lag effect, it is more evident for certain events than others. The time lag is quite evident in 2003. The spatial dimension also captures the time lag. For instance, after the end of the meteorological drought in April 2019, an extreme drought persisted in the surface and subsurface at a 12-month scale (section 6.2).

An additional aspect that also requires further investigation is the definition of the most appropriate time scale for drought monitoring. As explained in section 6.2, the onsets in meteorological and hydrological droughts would be different depending on the selected time scale. For instance, in the event of 1996, the hydrological drought started one month earlier than the meteorological drought based on a 9-month average. This finding would go against the concept of drought propagation. However, at shorter time scales, meteorological drought started first. On the other hand, a better agreement higher *r* coefficients and lower *RMSE* between modeled and in-situ PR and higher *r* coefficient for PR-ET anomalies were observed in medium and long time scales from 9 to 24 month-average. Regarding SM, no concluding remarks can be made due to the short in-situ time series.

Based on the analysis of the extreme droughts (taken from a 9-month scale reference) that occurred in 1996, 2003, and 2018, it is more likely that the trigger of the droughts are higher PR anomalies associated with higher PR-ETa rates. Regarding the performance of TSMP dataset to characterize droughts, we can conclude that it was more consistent at defining the duration of the phenomena and providing an acceptable description of the patterns, mostly in the SM and hydrological domains. Although, it was not accurate at determining the dates of the onset and end of the events and their associated intensities (section 6.3).

Finally, the performance of the dataset was fairly good at determining the areas more prone to extreme droughts. It was found that the SW, the North in the coastline of the Ijsselmeer, and a NE strip show a higher probability of drought occurrence at different time scales. The assessment carried out on a 9-month scale suggests that the TSMP inspection of critical areas was satisfactory, except for the Northern part (section 6.4).

To conclude, TSMP can be used to conduct a country-scale drought assessment by looking at the three different types of droughts. The analysis indicates that the dataset is more accurate at determining the most affected areas or areas with higher drought probability than providing a detailed assessment of a single drought.

LIST OF REFERENCES

Benninga, H. J. F., Carranza, C. D. U., Pezij, M., Van Santen, P., Van Der Ploeg, M. J., Augustijn, D. C. M., & Van Der Velde, R. (2018). The Raam regional soil moisture monitoring network in the Netherlands. *Earth System Science Data*, *10*(1), 61–79. https://doi.org/10.5194/essd-10-61-2018

Buitink, J., Swank, A. M., Van Der Ploeg, M., Smith, N. E., Benninga, H. J. F., Van Der Bolt, F., Carranza, C. D. U., Koren, G., Van Der Velde, R., & Teuling, A. J. (2020). Anatomy of the 2018 agricultural drought in the Netherlands using in situ soil moisture and satellite vegetation indices. *Hydrology and Earth System Sciences*, *24*(12), 6021–6031. https://doi.org/10.5194/hess-24-6021-2020

Dente, L., Vekerdy, Z., Su, Z., & Ucer, M. (2011). *Twente soil moisture and soil temperature monitoring network*. University of Twente, Faculty of Geo-Information Science and Earth Observation (ITC). http://www.itc.nl/library/papers_2011/scie/dente_twe.pdf

Furusho-Percot, C., Goergen, K., Hartick, C., Kulkarni, K., Keune, J., & Kollet, S. (2019). Pan-European groundwater to atmosphere terrestrial systems climatology from a physically consistent simulation. *Scientific Data*, *6*(1), 320. https://doi.org/10.1038/s41597-019-0328-7

Haarsma, R. J., Selten, F., van der Hurk, B., Hazeleger, W., & Wang, X. (2009). Drier Mediterranean soils due to greenhouse warming bring easterly winds over summertime central Europe. *Geophysical Research Letters*, *36*(4), 1–7. https://doi.org/10.1029/2008GL036617

Hartick, C., Furusho-Percot, C., Goergen, K., & Kollet, S. (2021). An Interannual Probabilistic Assessment of Subsurface Water Storage Over Europe Using a Fully Coupled Terrestrial Model. *Water Resources Research*, *57*(1). https://doi.org/10.1029/2020WR027828

Homdee, T., Pongput, K., & Kanae, S. (2016). A comparative performance analysis of three standardized climatic drought indices in the Chi River basin, Thailand. *Agriculture and Natural Resources*, *50*(3), 211–219. https://doi.org/10.1016/j.anres.2016.02.002

Keune, J., Gasper, F., Goergen, K., Hense, A., Shrestha, P., Sulis, M., & Kollet, S. (2016). Studying the influence of groundwater representations on land surface-atmosphere feedbacks during the European heat wave in 2003. *Journal of Geophysical Research*, *121*(22), 13,301-13,325. https://doi.org/10.1002/2016JD025426

KNMI. (2020). Explanation about drought. https://www.knmi.nl/kennis-en-datacentrum/uitleg/droogte

Maina, M. P. (2018). *Drought Monitoring and Assessment Using Remote Sensing* [Msc. dissertation, University of Twente]. University of Twente thesis repository. https://essay.utwente.nl/83345/

Mckee, T. B., Doesken, N. J., & Kleist, J. (1993). The relationship of drought frequency and duration to time scales. In: Proceedings of the Ninth Conference on Applied Climatology. *American Metereological Society*, *Boston*, 179–184.

Philip, S. Y., Kew, S. F., van der Wiel, K., Wanders, N., & van Oldenborgh, G. J. (2020). Regional differentiation in climate change induced drought trends in the Netherlands. *Environmental Research Letters*, *15*(9). https://doi.org/10.1088/1748-9326/ab97ca

Rehana, S., & Monish, N. T. (2020). Characterization of Regional Drought Over Water and Energy Limited Zones of India Using Potential and Actual Evapotranspiration. *Earth and Space Science*, *7*(10). https://doi.org/10.1029/2020EA001264

Sivakumar, M. V. K., Stefanski, R., Bazza, M., Zelaya, S., Wilhite, D., & Magalhaes, A. R. (2014). High Level meeting on national drought policy: Summary and major outcomes. *Weather and Climate Extremes*, *3*, 126–132. https://doi.org/10.1016/j.wace.2014.03.007

Stagge, J. H., Tallaksen, L. M., Gudmundsson, L., Van Loon, A. F., & Stahl, K. (2015). Candidate Distributions for Climatological Drought Indices (SPI and SPEI). *International Journal of Climatology*, *35*(13), 4027–4040. https://doi.org/10.1002/joc.4267

Su, Z., He, Y., Dong, X., & Wang, L. (2017). *Drought Monitoring and Assessment Using Remote Sensing. In V. Lakshmi (Ed.), Remote sensing of hydrological extremes (pp. 151-172). (Springer Remote Sensing / Photogrammetry). Springer. https://doi.org/10.1007/978-3-319-43744-6_8*

Van Der Velde, R., Colliander, A., Pezij, M., Benninga, H. J. F., Bindlish, R., Chan, S. K., Jackson, T. J., Hendriks, D. M. D., Augustijn, D. C. M., & Su, Z. (2021). Validation of SMAP L2 passive-only soil moisture products using upscaled in situ measurements collected in Twente, the Netherlands. *Hydrology and Earth System Sciences*, *25*(1), 473–495. https://doi.org/10.5194/hess-25-473-2021

Weijers, R. (2020). *Drought indicators in The Netherlands*. [Msc. dissertation, TU Delft]. TU Delft repositories. https://repository.tudelft.nl/islandora/object/uuid%3A3c915a71-95ee-462d-99fc-eaa2fd167765

WMO. (2012). *Standardized Precipitation Index User Guide* (WMO publication, No. 1090). https://library.wmo.int/?lvl=notice_display&id=13682#.YM3OC2j7RPY

Zhang, L. (2020). *Towards Long-term In-situ Based Gridded Soil Moisture Data at Global Scale using Random Forest Regression*. [Unpublished msc. dissertation]. University of Twente.